

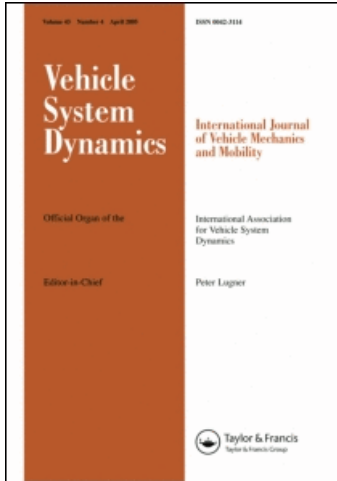
This article was downloaded by: [Malvezzi, Monica]

On: 11 May 2011

Access details: Access Details: [subscription number 937484129]

Publisher Taylor & Francis

Informa Ltd Registered in England and Wales Registered Number: 1072954 Registered office: Mortimer House, 37-41 Mortimer Street, London W1T 3JH, UK



Vehicle System Dynamics

Publication details, including instructions for authors and subscription information:

<http://www.informaworld.com/smpp/title~content=t713659010>

Development and implementation of a differential elastic wheel-rail contact model for multibody applications

E. Meli^a; S. Magheri^a; M. Malvezzi^b

^a Department of Energy Engineering, University of Florence, Firenze, Italy ^b Department of Information Engineering, University of Siena, Siena, Italy

First published on: 24 February 2011

To cite this Article Meli, E. , Magheri, S. and Malvezzi, M.(2011) 'Development and implementation of a differential elastic wheel-rail contact model for multibody applications', *Vehicle System Dynamics*, 49: 6, 969 — 1001, First published on: 24 February 2011 (iFirst)

To link to this Article: DOI: 10.1080/00423114.2010.504854

URL: <http://dx.doi.org/10.1080/00423114.2010.504854>

PLEASE SCROLL DOWN FOR ARTICLE

Full terms and conditions of use: <http://www.informaworld.com/terms-and-conditions-of-access.pdf>

This article may be used for research, teaching and private study purposes. Any substantial or systematic reproduction, re-distribution, re-selling, loan or sub-licensing, systematic supply or distribution in any form to anyone is expressly forbidden.

The publisher does not give any warranty express or implied or make any representation that the contents will be complete or accurate or up to date. The accuracy of any instructions, formulae and drug doses should be independently verified with primary sources. The publisher shall not be liable for any loss, actions, claims, proceedings, demand or costs or damages whatsoever or howsoever caused arising directly or indirectly in connection with or arising out of the use of this material.

Development and implementation of a differential elastic wheel–rail contact model for multibody applications

E. Meli^a, S. Magheri^a and M. Malvezzi^{b*}

^aDepartment of Energy Engineering, University of Florence, via S. Marta n. 3, 50139 Firenze, Italy;

^bDepartment of Information Engineering, University of Siena, via Roma n. 56, 53100 Siena, Italy

(Received 21 December 2009; final version received 09 June 2010; first published 24 February 2011)

The wheel–rail contact analysis plays a fundamental role in the multibody modelling of railway vehicles. A good contact model must provide an accurate description of the global and local contact phenomena (contact forces, position and shape of the contact patch, stresses and displacements) and a general handling of the multiple contact. The model has also to assure high numerical efficiency (in order to be implemented directly online within multibody models) and a good compatibility with commercial multibody software (Simpack Rail, Adams Rail). In this work, an elastic wheel–rail contact model that satisfies the previous specifics is presented. The model considers the wheel and the rail as elastic deformable bodies and requires the numerical solution of Navier's elasticity equation. The contact between wheel and rail has been described by means of suitable analytical contact conditions. Subsequently, the contact model has been inserted within the multibody model of a benchmark railway vehicle (the Manchester Wagon) in order to obtain a complete model of the wagon. The model has been implemented in the Matlab/Simulink environment. Finally, numerical simulations of the vehicle dynamics have been carried out on many different railway tracks with the aim of evaluating the performances of the model. The results obtained with the proposed method have been compared with those obtained by means of a standard commercial software. The main purpose is to achieve a better integration between the differential modelling and the multibody modelling. This kind of integration is almost absent in the literature (especially in the railway field) due to the computational cost and to the memory storage needs. However, it is very important because only the differential modelling allows an accurate analysis of the contact problem (in terms of contact forces, position and shape of the contact patch, stresses and displacements) while the multibody modelling is currently the standard in the study of the railway dynamics.

Keywords: multibody modelling; wheel–rail contact; contact between elastic bodies

1. Introduction

The multibody simulation of the railway vehicle dynamics needs a reliable contact model that satisfies the following requirements:

- (1) accurate description of the global and local contact phenomena (contact forces, position and shape of the contact patch, stresses and displacements);
- (2) general and accurate handling of multiple contact points;

*Corresponding author. Email: malvezzi@dii.unisi.it, malvezzi@mapp1.de.unifi.it

- (3) high computational efficiency (in order to be implemented directly online within multibody models);
- (4) compatibility with commercial multibody softwares (Simpack Rail, Adams Rail).

The wheel–rail contact problem has been discussed by several authors and many models can be found in the literature. Currently, the main multibody approaches to the problem are the so-called rigid contact formulation and the semi-elastic contact description. The rigid approach considers the wheel and the rail as rigid bodies. The contact is imposed by means of constraint equations and the contact points are detected during the dynamic simulation by solving the nonlinear algebraic differential equations associated with the constrained multibody system. Indentation between the bodies is not permitted and the normal contact forces are calculated through the Lagrange multipliers. Finally, Hertz's and Kalker's theories allow to evaluate the shape of the contact patch and the tangential forces, respectively [1–6].

Also the semi-elastic approach considers the wheel and the rail as rigid bodies. However, in this case, no kinematic constraints are imposed and the indentation between the bodies is permitted. The contact points are detected by means of approximated procedures (based on look-up tables and simplifying hypotheses on the problem geometry) or by means of semi-analytical methods (based on the reduction of the problem dimension). The normal contact forces are calculated as a function of the indentation, while, as in the rigid approach, Hertz's and Kalker's theories allow us to evaluate the shape of the contact patch and the tangential forces [4–10].

Both the described approaches are computationally very efficient but their generality and accuracy turn out to be often insufficient because the physical hypotheses behind these theories are too restrictive and, in many circumstances, unverified.

In order to obtain a complete description of the contact phenomena, differential contact models are needed. In other words, wheel and rail have to be considered as elastic bodies modelled by Navier's equations and the contact has to be described by suitable analytical contact conditions. The contact between elastic bodies has been widely studied in the literature both in the general case and in the rolling case. Many procedures based on variational inequalities, FEM techniques and convex optimisation have been developed. This kind of approach assures high generality and accuracy but still needs very large computational costs and memory consumption [4,11–17].

Owing to the required high computational load, referring to the current state of the art, the integration between multibody and differential modelling is not frequent in the literature, especially in the railway field [18]. However, this integration is very important because only the differential modelling allows an accurate analysis of the contact problem (in terms of contact forces, position and shape of the contact patch, stresses and displacements) while the multibody modelling is the standard in the study of the railway dynamics.

In this work, a differential contact model is presented, with the aim of achieving a better integration between multibody and differential modelling. The new contact model is fully 3D and satisfies all the requirements described above. The developed procedure needs the discretisation of the elastic contact problem (Navier's equations and analytical contact condition) and subsequently the solution of the nonlinear discrete problem. Both the steps have been implemented in Matlab/Simulink environment [19].

Then the contact model has been integrated with a 3D multibody model of a railway vehicle to obtain a complete model of the wagon. The railway vehicle chosen as benchmark is the Manchester Benchmark Vehicle, the physical and geometrical characteristics of which are easily available in the literature [20]. The multibody model has been implemented in SimMechanics, a Matlab toolbox specifically designed for multibody dynamics [19].

The 3D multibody model of the same vehicle (this time equipped with a standard contact model based on the semi-elastic approach) has been then implemented also in Simpack Rail, a commercial multibody software for railway vehicles widely tested and validated [21].

Finally, numerical simulations of the vehicle dynamics have been carried out on many different railway tracks with the aim of evaluating the performances of the whole model. The comparison between the results obtained by the Matlab/Simulink model and those obtained by the Simpack Rail model has allowed an accurate and reliable validation of the new contact model.

The paper is organised as follows. Section 2 describes the general architecture and how the contact model is integrated with the multibody model, Section 3 introduces the mathematical notation and the reference systems used to explain, in Section 4, the proposed differential contact model. Section 5 describes the features of the modelled vehicle that is used to perform numerical tests whose results and the comparison with those obtained with a standard commercial software are summarised in Section 6. Finally, Section 7 draws some conclusions on the proposed method.

2. General architecture of the model

As said in Section 1, the whole model consists of two different parts: the 3D multibody model of the railway vehicle (the Manchester Wagon [20]) and the 3D differential wheel–rail contact model. The general architecture of the model is schematically shown in the block diagram in Figure 1.

During the simulation, the multibody model interacts directly online with the differential contact model. At each time integration step, the multibody model evaluates the kinematic variables relative to the wheelset and consequently to each wheel–rail contact pair. Starting from these quantities, the contact model, based on Navier’s equations and suitable analytical contact conditions, calculates the global and local contact variables (forces, contact areas, stresses and displacements). The contact variables are then passed to the multibody model in order to carry on the simulation of the vehicle dynamics.

The differential contact model has been implemented in the Matlab/Simulink environment while the multibody model has been implemented in SimMechanics [19].

3. Reference systems and railway track

In this section, the mathematical notation concerning the reference systems and the railway track will be introduced [22–24]. The adopted reference systems are the same as described

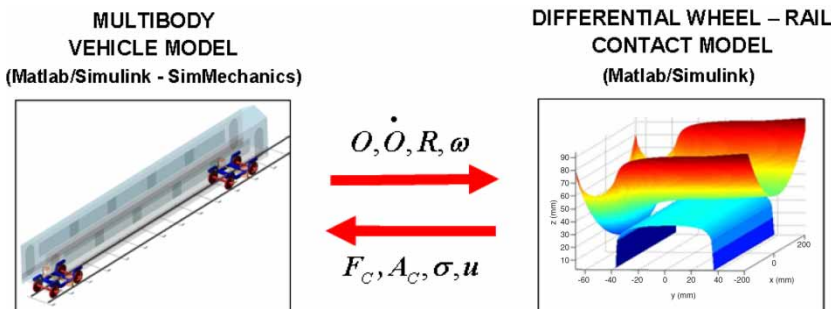


Figure 1. General architecture of the model.

in some preceding works [8–10]. However, in order to clarify the explanation, they are summarised in this section. First of all a *fixed reference system* $O_f x_f y_f z_f$ (Figure 2) is defined: the x_f axis is tangent to the centreline in the point O_f and the z_f axis is normal to the plane of the rails.

With respect to this base system, the railway track can be described by means of a three-dimensional curve:

$$\gamma(s) : I \subset R \rightarrow R^3, \tag{1}$$

where s is the curvilinear abscissa of γ (Figure 2). For convenience, we define $\tilde{\gamma}(s')$ as the projection of $\gamma(s)$ on the plane $x_f y_f$ (here s' is the curvilinear abscissa of $\tilde{\gamma}$). Usually, in the cartographic description of a railway track, only the curvature $K(s')$ of $\tilde{\gamma}$ and the track slope $p(s')$ are known; anyway, these parameters are sufficient to reconstruct the three-dimensional track. The curve $\tilde{\gamma}$ can be calculated directly from its curvature $K(s')$. The Frenet equations for $\tilde{\gamma}$ are:

$$\frac{d\mathbf{T}}{ds'} = K(s')\mathbf{N}, \quad \frac{d\mathbf{N}}{ds'} = -K(s')\mathbf{T}, \tag{2}$$

where $\mathbf{T}(s')$ and $\mathbf{N}(s')$ are, respectively, the tangent and the normal unitary vectors of the curve $\tilde{\gamma}$. Starting from the initial conditions $\mathbf{T}(0) = (1, 0)^T$ and $\mathbf{N}(0) = (0, 1)^T$, the Frenet equations can be integrated, obtaining $\mathbf{T}(s')$ and $\mathbf{N}(s')$. Then, since $\mathbf{T}(s') = ((d\tilde{\gamma}(s'))/ds')$, $\tilde{\gamma}(s')$ can be determined by integration:

$$\tilde{\gamma}(s') = \int_0^{s'} \mathbf{T}(u) du. \tag{3}$$

The track altitude $h(s')$ can be instead calculated using the definition of the track slope $p(s')$:

$$h(s') = \int_0^{s'} p(u) du. \tag{4}$$

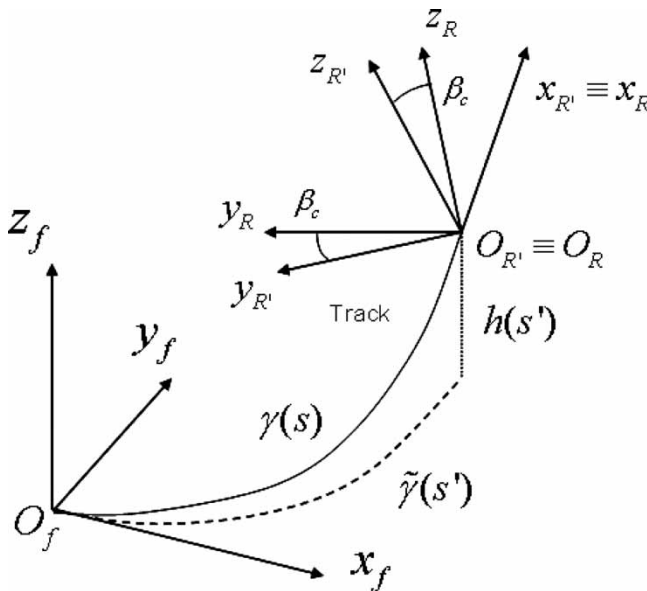


Figure 2. Fixed and auxiliary reference systems.

The track curve, as a function of the abscissa s' , has consequently the form

$$\bar{\gamma}(s') = \begin{pmatrix} \tilde{\gamma}(s') \\ h(s') \end{pmatrix}. \tag{5}$$

In order to obtain the expression of $\gamma(s)$, a relation between s and s' has to be established. Since s is the curvilinear abscissa of γ , the following equation holds:

$$s(s') = \int_0^{s'} \left\| \frac{d\bar{\gamma}(t)}{dt} \right\| dt = \int_0^{s'} \left\| \begin{pmatrix} \mathbf{T}(t) \\ p(t) \end{pmatrix} \right\| dt = \int_0^{s'} \sqrt{1 + p(t)^2} dt. \tag{6}$$

Obviously if $p(s') = 0$, $s = s'$. The relation $s(s')$ can be numerically inverted and inserted in expression (5):

$$\bar{\gamma}(s') = \bar{\gamma}(s'(s)) = \gamma(s). \tag{7}$$

A second reference system, referred as *auxiliary reference system* $O_R x_R y_R z_R$ (Figures 2 and 3) is introduced. It is placed on the plane of the rails and follows the motion of the wheelset during the simulation.

The x_R axis is tangent to the centreline in the point O_R and the z_R axis normal to the plane of the rails. The position of O_R can be calculated starting from the position of the centre of mass G (coincident with the wheelset reference system origin O_W , which will be described later) of the wheelset imposing the following condition:

$$(\mathbf{O}_W^f - \mathbf{O}_R^f) \cdot \mathbf{i}_R = (\mathbf{G}^f - \gamma(s)) \cdot \frac{d\gamma(s)}{ds} = 0 \tag{8}$$

and solving it with respect to the variable s . This condition is equivalent to impose that the plane $y_R z_R$ contains the point G .

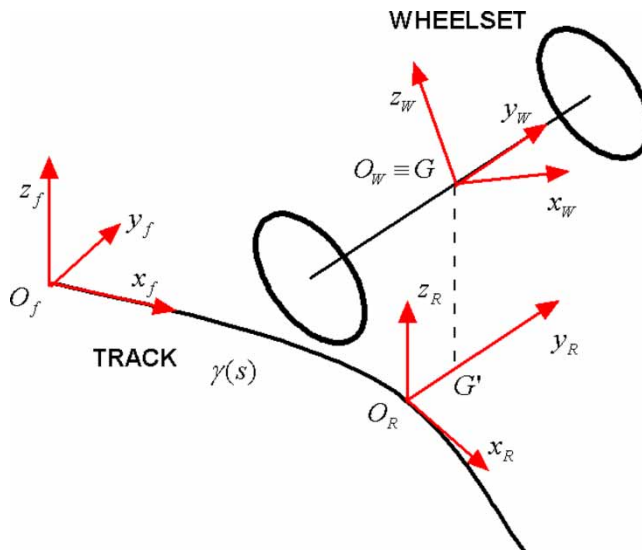


Figure 3. Fixed, auxiliary and local reference systems.

In order to define the axes y_R and z_R another reference system $O'_R x'_R y'_R z'_R$ is defined; its origin O'_R coincides with O_R while its unitary vectors can be evaluated as follows (Figure 2):

$$\mathbf{i}'_R = \mathbf{i}_R = \frac{d\gamma(s)}{ds}, \quad \mathbf{j}'_R = \mathbf{k}_f \wedge \mathbf{i}'_R, \quad \mathbf{k}'_R = \mathbf{i}'_R \wedge \mathbf{j}'_R. \tag{9}$$

The unitary vectors of the auxiliary system, expressed in the fixed reference system, are:

$$[\mathbf{i}_R \quad \mathbf{j}_R \quad \mathbf{k}_R] = R_{\text{cant}}[\mathbf{i}'_R \quad \mathbf{j}'_R \quad \mathbf{k}'_R], \tag{10}$$

where the rotation matrix R_{cant} is defined as:

$$R_{\text{cant}} = R_x(\beta_c) = \begin{pmatrix} 1 & 0 & 0 \\ 0 & \cos \beta_c & -\sin \beta_c \\ 0 & \sin \beta_c & \cos \beta_c \end{pmatrix}, \tag{11}$$

where β_c is the track cant angle.

Finally the *local reference system* $O_W x_W y_W z_W$ is defined. The y_W axis is coincident with the rotation axis of the wheelset, the origin O_W coincides with the centre of mass G and the x_W axis is contained in the plane $x_R y_R$. The local system is rigidly connected to the wheelset except for the rotation around its axis.

In order to describe the differential contact model correctly, two further reference systems have to be introduced for each wheel–rail pair: the *wheel system* and the *rail system*. For the sake of simplicity, only the left pair is shown in Figure 4.

The first system $O_w x_w y_w z_w$ is parallel to the system $O_W x_W y_W z_W$ and its origin O_w lies on the symmetry axis y_W of the wheel (Figure 5). Moreover, the origin O_w belongs to the nominal rolling plane, i.e. the plane normal to the rotation axis containing the nominal rolling radius [22]. The second system $O_r x_r y_r z_r$ is parallel to the system $O_R x_R y_R z_R$ (Figure 5). Its origin O_r belongs to the axis y_R while the distance between O_R and O_r has to assure the correct gauge between the rails [22]. The global and local contact variables will be evaluated by the contact model with respect to these reference systems. For the numerical simulations presented in the following sections, two standard profiles have been considered: the UIC 60 for the rails (here α_p is the laying angle) and the ORE S 1002 for the wheels (Figure 6) [22].

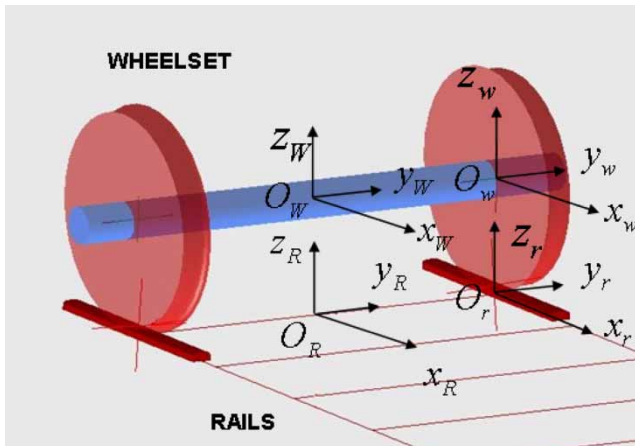


Figure 4. Wheel and rail reference systems.

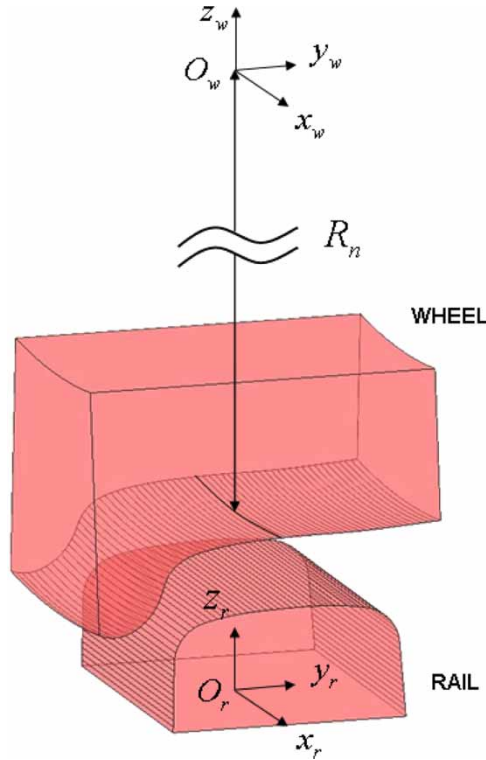


Figure 5. Location of the wheel and rail systems.

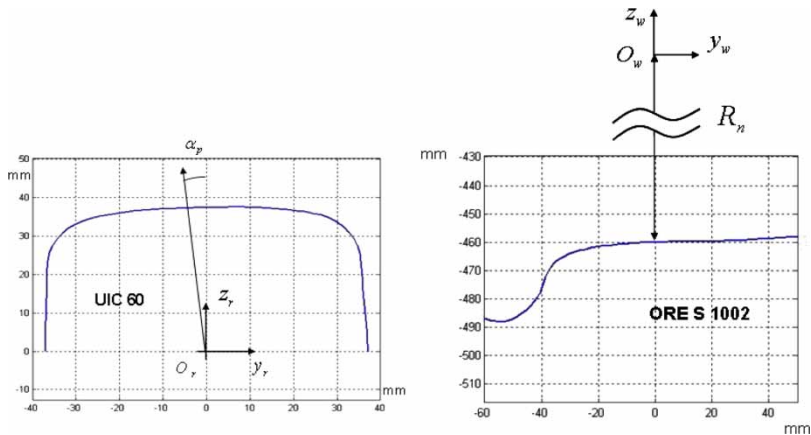


Figure 6. Wheel and rail profiles.

4. The differential wheel–rail contact model

In this section, the 3D differential wheel–rail contact model will be described. For the sake of simplicity, as regards the generic contact variable Z , the following convention will be adopted: Z_w and Z_w^r will denote a variable relative to the wheel, respectively, expressed in the reference

systems $O_w x_w y_w z_w$ and $O_r x_r y_r z_r$ while Z_r^w and Z_r will denote a variable relative to the rail expressed in the same systems.

With reference to Figure 1, the contact model can be thought of as a *black box* having the following inputs and outputs.

- *Inputs*: the kinematic variables relative to the considered wheel–rail pair (in this case, the left one), i.e. the position O_w^r , the orientation R_w^r , the absolute velocity \dot{O}_w^r and the absolute angular velocity ω_w^r of the *wheel system* and the analogous quantities of the *rail system* $O_r = \mathbf{0}$, $R_r = I$, \dot{O}_r and ω_r (Figures 4 and 5).
- *Outputs*: the global and local contact variables relative to the wheel and to the rail, like the contact forces F_{wC} and F_{rC} , the contact patches A_{wC} and A_{rC} , the stresses σ_w and σ_r and the displacements u_w and u_r .

4.1. The kinematics of the problem

The wheel and the rail have been considered as two linear elastic bodies Ω_w and Ω_r (as shown in Figure 7). Both the domains are supposed to be large enough with respect to the dimensions of the contact patch [13,14].

The boundaries $\partial\Omega_w$ and $\partial\Omega_r$ are split into two disjoint regions, respectively, Γ_{wC} , Γ_{wD} and Γ_{rC} , Γ_{rD} . The contact boundaries Γ_{wC} and Γ_{rC} (dashed in Figure 7) are the regions where the contact may verify while on the Dirichlet boundaries Γ_{wD} and Γ_{rD} the displacements are known and equal to zero. The knowledge of the wheel–rail kinematics (see the inputs of the contact model) and consequently of the location of the Dirichlet boundaries has been used, during the simulation, to determine the position of the undeformed configurations.

In case of contact, the geometric intersection between the surfaces Γ_{wC} and Γ_{rC} (and thus between the undeformed configurations) allows us to define the penetration areas $\tilde{A}_{wC} \subset \Gamma_{wC}$ and $\tilde{A}_{rC} \subset \Gamma_{rC}$ (with $\tilde{A}_{wC} \approx \tilde{A}_{rC}$) that can be considered as a first rough estimate of the real contact areas A_{wC} and A_{rC} . The situation is schematically sketched in Figures 7 and 8.

The real contact areas $A_{wC} \subset \tilde{A}_{wC}$ and $A_{rC} \subset \tilde{A}_{rC}$ (with $A_{wC} \approx A_{rC}$) are unknown and have to be calculated by the model. For this purpose, a contact map Φ has to be introduced. The contact map $\Phi : \tilde{A}_{wC} \rightarrow \tilde{A}_{rC}$ (by convention the wheel is the master body) connects the generic point $x_w^r \in \tilde{A}_{wC}$ on the wheel surface with the point $\Phi(x_w^r) \in \tilde{A}_{rC}$ on the rail surface

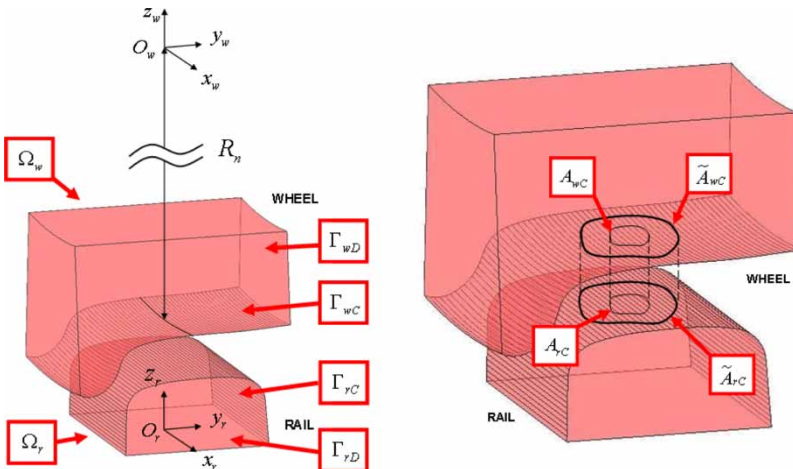


Figure 7. Domains, boundaries and contact areas.

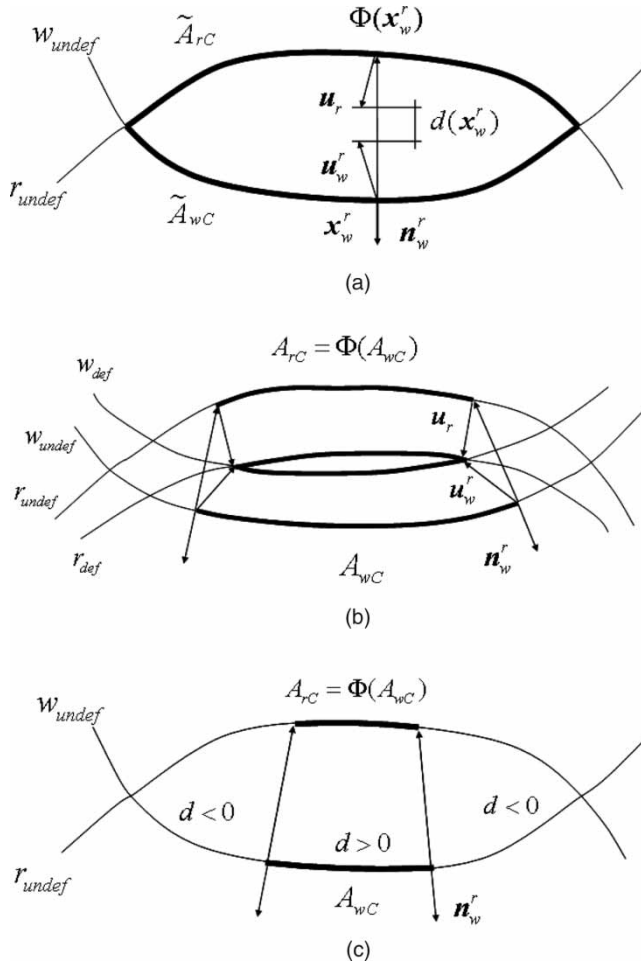


Figure 8. Contact map and distance function.

that will get in contact with the point on the wheel surface in the deformed configuration. In this case the map Φ is defined as the normal projection $\Phi(\mathbf{x}_w^r)$ of the point $\mathbf{x}_w^r \in \tilde{A}_{wC}$ on the surface \tilde{A}_{rC} . Starting from the contact map, the distance function between the deformed configurations $d : \tilde{A}_{wC} \rightarrow R$ can be evaluated:

$$d(\mathbf{x}_w^r) = (\mathbf{u}_w^r - \mathbf{u}_r) \cdot \mathbf{n}_w^r - (\Phi(\mathbf{x}_w^r) - \mathbf{x}_w^r) \cdot \mathbf{n}_w^r \quad (12)$$

where \mathbf{n}_w^r is the outgoing normal versor to the surfaces Γ_{wC} . The function d is positive if there is penetration between the deformed configurations and negative otherwise (Figure 8).

Formally, the contact area A_{wC} is defined as the region of \tilde{A}_{wC} , where the function d is positive while the contact area $A_{rC} = \Phi(A_{wC})$ is the normal projection of A_{wC} on \tilde{A}_{rC} . In other words, from a kinematic point of view, the penetration between the deformed bodies is allowed and will have to be penalised by the contact model (Figure 8) [13,14].

In this way, the estimated contact areas \tilde{A}_{wC} and \tilde{A}_{rC} depend only on the relative wheel - rail kinematics ($\mathbf{O}_w^r, R_w^r, \dot{\mathbf{O}}_w^r, \omega_w^r$ and $\dot{\mathbf{O}}_r, \omega_r$) while the real contact areas A_{wC} and A_{rC} depend also on the displacements \mathbf{u}_w and \mathbf{u}_r . Finally, it is useful to remark that no hypothesis has been

made on the shape of the contact patch; in particular, the contact area can be made up of one or more disjoint parts.

4.2. The contact model

According to the linear theory of elasticity [13,14], the wheel and the rail stresses σ_w and σ_r are governed by Navier’s equations:

$$\begin{aligned}
 \operatorname{div} \sigma_w(\mathbf{u}_w) &= \mathbf{0} && \text{on } \Omega_w \\
 \operatorname{div} \sigma_r(\mathbf{u}_r) &= \mathbf{0} && \text{on } \Omega_r \\
 \mathbf{u}_w &= \mathbf{0} && \text{on } \Gamma_{wD} \\
 \mathbf{u}_r &= \mathbf{0} && \text{on } \Gamma_{rD} \\
 \sigma_w(\mathbf{u}_w)\mathbf{n}_w &= \mathbf{p}_w && \text{on } \tilde{A}_{wC} \\
 \sigma_w(\mathbf{u}_w)\mathbf{n}_w &= \mathbf{0} && \text{on } \Gamma_{wC} \setminus \tilde{A}_{wC} \\
 \sigma_r(\mathbf{u}_r)\mathbf{n}_r &= \mathbf{p}_r && \text{on } \tilde{A}_{rC} \\
 \sigma_r(\mathbf{u}_r)\mathbf{n}_r &= \mathbf{0} && \text{on } \Gamma_{rC} \setminus \tilde{A}_{rC},
 \end{aligned}
 \tag{13}$$

where \mathbf{n}_w and \mathbf{n}_r are the outgoing normal vectors to the surfaces Γ_{wC} and Γ_{rC} while \mathbf{p}_w and \mathbf{p}_r are the unknown contact pressures. The pressures \mathbf{p}_w and \mathbf{p}_r are defined on \tilde{A}_{wC} and \tilde{A}_{rC} but will have to be zero on $\tilde{A}_{wC} \setminus A_{wC}$ and $\tilde{A}_{rC} \setminus A_{rC}$. For both the contact bodies, the characteristics of the steel (Young’s modulus $E_w = E_r = 2.1 * 10^{11}$ Pa and Poisson’s coefficient $\nu_w = \nu_r = 0.3$) have been considered.

In the presented case, volume forces (i.e. the gravity) and inertial terms have been neglected because their influence on the contact phenomena is negligible, but of course they have to be considered in the multibody model of the railway vehicle. Moreover, the problem is supposed to be steady within the time integration step [4,13,14].

Equivalently, problem (13) can be formulated in a weak form as follows:

$$\begin{aligned}
 \int_{\Omega_w} \sigma_w(\mathbf{u}_w) : \varepsilon_w(\mathbf{v}_w) dV &= \int_{\tilde{A}_{wC}} \mathbf{p}_w \cdot \mathbf{v}_w dA \quad \forall \mathbf{v}_w \in V_w \\
 \int_{\Omega_r} \sigma_r(\mathbf{u}_r) : \varepsilon_r(\mathbf{v}_r) dV &= \int_{\tilde{A}_{rC}} \mathbf{p}_r \cdot \mathbf{v}_r dA \quad \forall \mathbf{v}_r \in V_r,
 \end{aligned}
 \tag{14}$$

where ε_w and ε_r are the strains while V_w and V_r are suitable Sobolev’s spaces [13,14].

In order to complete the contact model, the contact pressures \mathbf{p}_w and \mathbf{p}_r have to be expressed as a function of the displacements \mathbf{u}_w and \mathbf{u}_r . For the sake of simplicity, the normal and the tangential contact pressures on the wheel are introduced:

$$p_{wN}^r = \mathbf{p}_w^r \cdot \mathbf{n}_w^r \quad \mathbf{p}_{wT}^r = \mathbf{p}_w^r - p_{wN}^r \mathbf{n}_w^r.
 \tag{15}$$

The normal pressure p_{wN}^r has been calculated by means of the distance function d and has to penalise the penetration between the deformed configurations (as discussed in Section 4.1):

$$p_{wN}^r(\mathbf{x}_w^r) = -K \max(d(\mathbf{x}_w^r), 0) \quad \text{on } \tilde{A}_{wC},
 \tag{16}$$

where K is a fictitious stiffness constant. The value of K has to be chosen large enough to assure the accuracy required by this kind of problems. The condition of ideal contact (total

Downloaded By: [Malvezzi, Monica] At: 09:55 11 May 2011

absence of penetration between the deformed configurations) is reached for $K \rightarrow +\infty$ (usually $K \geq 10^{15} \text{ N/m}^3$) [13,14].

To evaluate the tangential pressure \mathbf{p}_{wT}^r , the slip \mathbf{s}_w^r between the wheel and rail surfaces has to be defined. Since the solution is supposed to be steady within the time integration step (Figure 1), the following expression holds [4,13,14]:

$$\begin{aligned} \mathbf{s}_w^r(\mathbf{x}_w^r) &= \mathbf{w}_w^r(\mathbf{x}_w^r) + \dot{\mathbf{u}}_w^r(\mathbf{x}_w^r) - \mathbf{w}_r(\Phi(\mathbf{x}_w^r)) - \dot{\mathbf{u}}_r(\Phi(\mathbf{x}_w^r)) = \\ &= \mathbf{w}_w^r(\mathbf{x}_w^r) + J_w^r(\mathbf{x}_w^r)\mathbf{w}_w^r(\mathbf{x}_w^r) - \mathbf{w}_r(\Phi(\mathbf{x}_w^r)) - J_r(\Phi(\mathbf{x}_w^r))\mathbf{w}_r(\Phi(\mathbf{x}_w^r)), \end{aligned} \quad (17)$$

where \mathbf{w}_w^r and \mathbf{w}_r are the absolute rigid velocities of the points \mathbf{x}_w^r and \mathbf{x}_r (computable starting from the knowledge of the wheel–rail kinematic variables $\mathbf{O}_w^r, R_w^r, \dot{\mathbf{O}}_w^r, \omega_w^r$ and \mathbf{O}_r, ω_r) while J_w^r and J_r are the Jacobians of \mathbf{u}_w^r and \mathbf{u}_r with respect to the variables \mathbf{x}_w^r and \mathbf{x}_r . As usual, the normal and the tangential slips are:

$$s_{wN}^r = \mathbf{s}_w^r \cdot \mathbf{n}_w^r \mathbf{s}_{wT}^r = s_w^r - s_{wN}^r \mathbf{n}_w^r. \quad (18)$$

According to the standard pseudo-Coulombian friction models, the tangential pressure \mathbf{p}_{wT}^r can be expressed as follows:

$$\mathbf{p}_{wT}^r(\mathbf{x}_w^r) = -\mu(\|\mathbf{s}_{wT}^r(\mathbf{x}_w^r)\|, V) |p_{wN}^r(\mathbf{x}_w^r)| \frac{\mathbf{s}_{wT}^r(\mathbf{x}_w^r)}{\|\mathbf{s}_{wT}^r(\mathbf{x}_w^r)\|} \quad \text{on } \tilde{A}_{wC}, \quad (19)$$

where V is the longitudinal velocity of the vehicle. Further details on the friction function $\mu(\|\mathbf{s}_{wT}^r(\mathbf{x}_w^r)\|, V)$ can be found in the literature [4,13,14,23].

Finally the action–reaction principle (Newton’s third law) allows us to calculate the pressures \mathbf{p}_r :

$$\mathbf{p}_r(\Phi(\mathbf{x}_w^r)) = -\mathbf{p}_w^r(\mathbf{x}_w^r) \quad \text{on } \tilde{A}_{wC}. \quad (20)$$

In conclusion it is useful to remark that, according to the described model, the contact pressures \mathbf{p}_w^r and \mathbf{p}_r are zero, respectively, on $\tilde{A}_{wC} \setminus A_{wC}$ and $\tilde{A}_{rC} \setminus A_{rC}$. The displacements \mathbf{u}_w and \mathbf{u}_r will be evaluated through the numerical solution of Equation (14). The knowledge of these unknown quantities will allow us to calculate all the other required outputs such as the contact areas A_{wC} and A_{rC} and the stresses σ_w and σ_r . The contact forces \mathbf{F}_{wC} and \mathbf{F}_{rC} will be estimated by integration:

$$\mathbf{F}_{wC} = \int_{\tilde{A}_{wC}} \mathbf{p}_w dA \quad \mathbf{F}_{rC} = \int_{\tilde{A}_{rC}} \mathbf{p}_r dA. \quad (21)$$

4.3. The discretisation of the model

Both the elastic bodies have been discretised by means of tetrahedral elements and linear shape functions. The meshes have been built according to the standard Delaunay’s algorithms (Figure 9) [15,17].

The resolution of the meshes on the surfaces Γ_{wC} and Γ_{rC} is constant because the position and the dimensions of the contact area are *a priori* unknown. Moreover, the surface resolution (usually in the range 0.1 – 1 mm) has to assure an accuracy enough to correctly describe the contact phenomena. It is important to remark that the meshes have been created directly in the reference systems $O_w x_w y_w z_w$ and $O_r x_r y_r z_r$; therefore they do not change during the simulation and can be easily built offline without increasing the computational load.

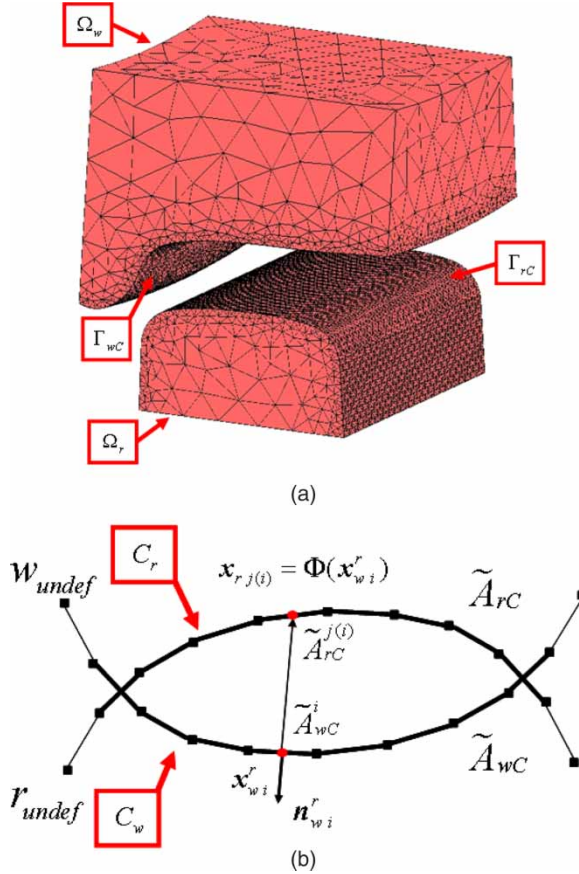


Figure 9. Discretisation of the Contact Model.

The following convention will be adopted.

- (1) The sets of the elements of wheel and rail will be called T_w and T_r while the vectors $\mathbf{u}_{wh}, \mathbf{u}_{rl} \in R^{12}$ will contain the displacements of the four nodes belonging to the elements $h \in T_w$ and $l \in T_r$. Finally, the vectors \mathbf{U}_w and \mathbf{U}_r will comprise the displacements relative to all the nodes of wheel and rail. Since the displacements on Γ_{wD} and Γ_{rD} are zero, the dimensions of $\mathbf{U}_w, \mathbf{U}_r$ are $3(N_w - N_{wD})$ and $3(N_r - N_{rD})$, where N_w and N_r are the numbers of nodes of wheel and rail while N_{wD} and N_{rD} are the numbers of nodes on Γ_{wD} and Γ_{rD} .
- (2) similarly $C_w \subset T_w$ and $C_r \subset T_r$ will be the sets of the active contact elements on wheel and on rail, i. e. the sets of the elements having respectively a face \tilde{A}_{wC}^i and \tilde{A}_{rC}^j that lies on \tilde{A}_{wC} and \tilde{A}_{rC} . The vectors $\mathbf{u}_{wi}, \mathbf{u}_{rj} \in R^{12}$ will contain the displacements of the four nodes belonging to the elements $i \in C_w$ and $j \in C_r$ while the vectors \mathbf{U}_{wC} and \mathbf{U}_{rC} will comprise the displacements relative to all the active elements. The dimension of $\mathbf{U}_{wC}, \mathbf{U}_{rC}$ are $3N_{wC}$ and $3N_{rC}$, where N_{wC} and N_{rC} are the number of nodes belonging to the active elements.

The knowledge of the wheel–rail kinematics ($\mathbf{O}_w^r, R_w^r, \dot{\mathbf{O}}_w^r, \omega_w^r$ and $\dot{\mathbf{O}}_r, \omega_r$) and consequently of the estimated contact areas \tilde{A}_{wC} and \tilde{A}_{rC} allows us to determine the sets C_w and C_r of the active contact elements on the wheel and on the rail.

For each active contact element on the wheel, the centre \mathbf{x}_{wi}^r of the face \tilde{A}_{wC}^i is considered. The normal projection $\mathbf{x}_{rj} = \Phi(\mathbf{x}_{wi}^r)$ of \mathbf{x}_{wi}^r on \tilde{A}_{rC} will belong to the external face \tilde{A}_{rC}^j of the j th active contact element on the rail; in particular, the index $j(i)$ will be a function of the index i . In this way, the pairs of points $(\mathbf{x}_{wi}^r, \mathbf{x}_{rj(i)})$ with $i \in C_w$ can be thought of as the discretisation of the contact map Φ . The situation is schematically sketched in Figure 9.

The values of the displacements $\mathbf{u}_w^r, \mathbf{u}_r$ and of their Jacobians $\mathbf{J}_w^r, \mathbf{J}_r$ in the points \mathbf{x}_{wi}^r and \mathbf{x}_{rj} are evaluated through the shape functions N_{wi}, N_{rj} :

$$\begin{aligned} \mathbf{u}_w^r(\mathbf{x}_{wi}^r) &= N_{wi}(\mathbf{x}_{wi}^r)\mathbf{u}_{wi}^r & J_w^r(\mathbf{x}_{wi}^r) &= \sum_{k=1}^{12} J_{wi}^k(\mathbf{x}_{wi}^r)u_{wik}^r \\ \mathbf{u}_r(\mathbf{x}_{rj}) &= N_{rj}(\mathbf{x}_{rj})\mathbf{u}_{rj} & J_r(\mathbf{x}_{rj}) &= \sum_{k=1}^{12} J_{rj}^k(\mathbf{x}_{rj})u_{rjk} \end{aligned} \tag{22}$$

where J_{wi}^k, J_{rj}^k are the Jacobians of the k th column of N_{wi} and N_{rj} while u_{wik}, u_{rjk} are the k th components of \mathbf{u}_{wi}^r and \mathbf{u}_{rj} [13–15,17].

At this point, the distance function $d_i = d(\mathbf{x}_{wi}^r)$ and the pressure $\mathbf{p}_{wi}^r = \mathbf{p}^r(\mathbf{x}_{wi}^r)$ on the face \tilde{A}_{wC}^i of the active element of the wheel can be calculated by means of Equations (12), (16) and (19). Finally, a discrete version of the action–reaction principle (the Newton’s third law) is needed to evaluate the pressure $\mathbf{p}_{rj(i)} = \mathbf{p}_r(\mathbf{x}_{rj(i)})$ on the face $\tilde{A}_{rC}^{j(i)}$ of the active element of the rail:

$$|\tilde{A}_{rC}^{j(i)}|\mathbf{p}_{rj(i)} = -|\tilde{A}_{wC}^i|\mathbf{p}_{wi}^r \tag{23}$$

where $|\tilde{A}_{wC}^i|$ and $|\tilde{A}_{rC}^{j(i)}|$ are the areas of the faces \tilde{A}_{wC}^i and $\tilde{A}_{rC}^{j(i)}$. Both the pressures \mathbf{p}_{wi}^r and $\mathbf{p}_{rj(i)}$ are supposed to be constant on \tilde{A}_{wC}^i and $\tilde{A}_{rC}^{j(i)}$.

Standard FEM techniques allow us to discretise the weak form of the contact problem (Equation (14)) [13–15,17]:

$$\begin{aligned} \int_{\Omega_w} \sigma_w(\mathbf{u}_w) : \varepsilon_w(\mathbf{v}_w) dV &= \sum_{h \in T_w} \mathbf{u}_{wh}^T K_{wh} \mathbf{v}_{wh} = \mathbf{U}_w^T K_w \mathbf{V}_w \\ \int_{\tilde{A}_{wC}} \mathbf{p}_w \cdot \mathbf{v}_w dA &= \sum_{i \in C_w} \mathbf{p}_{wi}^T M_{wi} \mathbf{v}_{wi} = \mathbf{F}_w(\mathbf{U}_{wC}, \mathbf{U}_{rC})^T \mathbf{V}_w \\ \int_{\Omega_r} \sigma_r(\mathbf{u}_r) : \varepsilon_r(\mathbf{v}_r) dV &= \sum_{l \in T_r} \mathbf{u}_{rl}^T K_{rl} \mathbf{v}_{rl} = \mathbf{U}_r^T K_r \mathbf{V}_r \\ \int_{\tilde{A}_{rC}} \mathbf{p}_r \cdot \mathbf{v}_r dA &= \sum_{i \in C_w} \mathbf{p}_{rj(i)}^T M_{rj(i)} \mathbf{v}_{rj(i)} = \mathbf{F}_r(\mathbf{U}_{wC}, \mathbf{U}_{rC})^T \mathbf{V}_r \end{aligned} \tag{24}$$

where K_{wh} and K_{rl} are the stiffness matrices relative to the elements $h \in T_w, l \in T_r$ and

$$M_{wi} = \int_{\tilde{A}_{wC}^i} N_{wi} dA \quad M_{rj(i)} = \int_{\tilde{A}_{rC}^{j(i)}} N_{rj(i)} dA. \tag{25}$$

The global stiffness matrices K_w and K_r are symmetric, positive defined and sparse while the vectors \mathbf{F}_w and \mathbf{F}_r , which contain the terms due to the contact pressures, are sparse. Moreover, also the global stiffness matrices are evaluated directly in the reference systems $O_w x_w y_w z_w$

and O_r, x_r, y_r, z_r ; therefore, they do not change during the simulation and can be easily built offline without increasing the computational load. Equations (14) and (24), combined together, give

$$\begin{aligned} \mathbf{U}_w^T K_w \mathbf{V}_w &= \mathbf{F}_w(\mathbf{U}_{wC}, \mathbf{U}_{rC})^T \mathbf{V}_w \quad \forall \mathbf{V}_w \in R^{3(N_w - N_{wD})} \\ \mathbf{U}_r^T K_r \mathbf{V}_r &= \mathbf{F}_r(\mathbf{U}_{wC}, \mathbf{U}_{rC})^T \mathbf{V}_r \quad \forall \mathbf{V}_r \in R^{3(N_r - N_{rD})}. \end{aligned} \tag{26}$$

Finally, since the matrices K_w, K_r are symmetric and the vectors $\mathbf{V}_w, \mathbf{V}_r$ are arbitrary, the following nonlinear system of algebraic equations is obtained:

$$\begin{aligned} K_w \mathbf{U}_w &= \mathbf{F}_w(\mathbf{U}_{wC}, \mathbf{U}_{rC}) \\ K_r \mathbf{U}_r &= \mathbf{F}_r(\mathbf{U}_{wC}, \mathbf{U}_{rC}) \end{aligned} \tag{27}$$

in which, as said before, the contact displacements $\mathbf{U}_{wC}, \mathbf{U}_{rC}$ are a subset of the displacements $\mathbf{U}_w, \mathbf{U}_r$. Equation (27) will be called the *sparse formulation* of the discrete contact problem. Equation (27) can be also written as

$$\begin{aligned} \mathbf{U}_w &= H_w \mathbf{F}_w(\mathbf{U}_{wC}, \mathbf{U}_{rC}) \\ \mathbf{U}_r &= H_r \mathbf{F}_r(\mathbf{U}_{wC}, \mathbf{U}_{rC}) \end{aligned} \tag{28}$$

where the matrices $H_w = K_w^{-1}$ and $H_r = K_r^{-1}$ are symmetric, positive defined and full. Like K_w and K_r , they do not change during the simulation and can be calculated offline (however, their storage can require an high memory consumption). Splitting $\mathbf{U}_w, \mathbf{U}_r$ into contact displacements $\mathbf{U}_{wC}, \mathbf{U}_{rC}$ and non-contact displacements $\mathbf{U}_{wNC}, \mathbf{U}_{rNC}$, Equation (28) becomes

$$\begin{aligned} \begin{pmatrix} \mathbf{U}_{wNC} \\ \mathbf{U}_{wC} \end{pmatrix} &= \begin{bmatrix} H_w^{11} & H_w^{12} \\ H_w^{21} & H_w^{22} \end{bmatrix} \begin{pmatrix} \mathbf{0} \\ \mathbf{f}_w(\mathbf{U}_{wC}, \mathbf{U}_{rC}) \end{pmatrix} \\ \begin{pmatrix} \mathbf{U}_{rNC} \\ \mathbf{U}_{rC} \end{pmatrix} &= \begin{bmatrix} H_r^{11} & H_r^{12} \\ H_r^{21} & H_r^{22} \end{bmatrix} \begin{pmatrix} \mathbf{0} \\ \mathbf{f}_r(\mathbf{U}_{wC}, \mathbf{U}_{rC}) \end{pmatrix}. \end{aligned} \tag{29}$$

In this way, the second and the fourth components of equation (29) are sufficient to calculate the contact displacements $\mathbf{U}_{wC}, \mathbf{U}_{rC}$:

$$\begin{aligned} \mathbf{U}_{wC} &= H_w^{22} \mathbf{f}_w(\mathbf{U}_{wC}, \mathbf{U}_{rC}) \\ \mathbf{U}_{rC} &= H_r^{22} \mathbf{f}_r(\mathbf{U}_{wC}, \mathbf{U}_{rC}). \end{aligned} \tag{30}$$

Equation (30) will be called the *reduced formulation* of the discrete contact problem. The matrices H_w^{22} and H_r^{22} have the same properties as H_w and H_r but this time their dimensions are much smaller. However, H_w^{22} and H_r^{22} change during the simulation and therefore have to be built directly online. The vectors \mathbf{f}_w and \mathbf{f}_r are full.

The remaining non-contact displacement $\mathbf{U}_{wNC}, \mathbf{U}_{rNC}$ can be evaluated by means of the first and the third components of Equation (29):

$$\begin{aligned} \mathbf{U}_{wNC} &= H_w^{12} \mathbf{f}_w(\mathbf{U}_{wC}, \mathbf{U}_{rC}) \\ \mathbf{U}_{rNC} &= H_r^{12} \mathbf{f}_r(\mathbf{U}_{wC}, \mathbf{U}_{rC}). \end{aligned} \tag{31}$$

The displacements $\mathbf{U}_w, \mathbf{U}_r$, evaluated by solving Equation (27) or Equation (30), allows us to calculate the contact areas A_{wC} and A_{rC} and the stresses σ_w and σ_r . The contact forces \mathbf{F}_{wC} and \mathbf{F}_{rC} are estimated by numerical integration:

$$\mathbf{F}_{wC} = \sum_{i \in C_w} |\tilde{A}_{wC}^i| \mathbf{p}_{wi} \quad \mathbf{F}_{rC} = \sum_{i \in C_w} |\tilde{A}_{rC}^{j(i)}| \mathbf{p}_{rj(i)}. \tag{32}$$

4.4. The numerical solution of the discrete problem

In this section, the numerical methods used for solving the discrete contact problem are presented. Both the *sparse formulation* (Equation (27)) and the *reduced formulation* (Equation (30)) will be analysed in the following.

Equation (27) is a large and sparse nonlinear system; on the contrary, Equation (30) is a full nonlinear system with much smaller dimensions than Equation (27). The typical dimensions of K_w and K_r (depending on the mesh resolution) are in the range $10^4 - 10^5$ while those of H_w^{22} and H_r^{22} (depending on the number of active elements) are about $10^2 - 10^3$.

Nonlinear solvers based on Newton–Krylov methods are usually very efficient for solving large and sparse systems like Equation (27) [25]. Newton–Krylov methods are Newton-type methods for the problem $\mathbf{F}(\mathbf{x}) = \mathbf{0}$, where \mathbf{F} is a generic nonlinear function. In particular, Krylov methods are employed to solve approximately the arising linear systems:

$$F'(\mathbf{x}_k)\mathbf{s}_k = -\mathbf{F}(\mathbf{x}_k), \quad (33)$$

where F' is the Jacobian of \mathbf{F} . The Krylov method computes, at each iteration, the so-called inexact Newton step $\tilde{\mathbf{s}}_k$ which satisfies the condition:

$$\|F'(\mathbf{x}_k)\tilde{\mathbf{s}}_k + \mathbf{F}(\mathbf{x}_k)\| \leq \eta_k \|\mathbf{F}(\mathbf{x}_k)\| \quad \eta_k \in [0, 1), \quad (34)$$

where the forcing terms η_k are used to control the level of accuracy [25]. In the studied case, a constant forcing term $\eta_k = \eta \leq 0.5 \forall k$ has been chosen while the method stops if the following stopping criterion is satisfied:

$$\|\mathbf{F}(\mathbf{x}_k)\| < \text{Tol}. \quad (35)$$

As regards the considered problem, numerical experimentations showed that, among all the Krylov methods, the best linear solver is the BiCGStab [26]. This particular kind of nonlinear solver is known as the Newton–BiCGStab method.

Iterative methods such as the BiCGStab often need a good preconditioner. The employed preconditioner P has been defined as follows:

$$P = \begin{pmatrix} K_w & 0 \\ 0 & K_r \end{pmatrix}. \quad (36)$$

Since Equation (27) is weakly nonlinear, the preconditioner P is a good approximation of the Jacobian. In general, the BiCGStab does not require the whole matrix P but only a factorisation of it. In the considered case, the incomplete Cholesky factorisation [26] has been used because the matrix P is not only symmetric and positive defined but also sparse. Moreover, this factorisation performs a reordering of P and takes advantage of its sparsity in terms of execution time and memory consumption.

An interesting feature of the Newton–BiCGStab method is that it requires only the action of F' on a vector \mathbf{v} but not the computation and the storage of the whole Jacobian. In this case, the product $F'(\mathbf{x})\mathbf{v}$ can be approximated by means of finite differences [27]:

$$F'(\mathbf{x})\mathbf{v} \approx \frac{\mathbf{F}(\mathbf{x} + \varepsilon\mathbf{v}) - \mathbf{F}(\mathbf{x})}{\varepsilon}, \quad (37)$$

where $\varepsilon > 0$ is a scalar small enough. Consequently, this method is called ‘matrix-free’.

The same nonlinear solver (Newton–BiCGStab), this time without preconditioner, has been used in order to solve Equation (30). In this circumstance, due to the small dimensions of the problem, the arising linear systems (33) can be also solved by means of direct methods (like the

LU method [28]). Therefore, a second nonlinear solver based on this kind of procedures (the Newton–LU method) has been analysed and experimented on system (30). The employment of this alternative approach needs the computation and the storage of the whole Jacobian F' at each nonlinear iteration.

Finally, it has to be remarked that, if the guarantee of convergence is only local, the nonlinear solvers (the Newton–BiCGStab and the Newton–LU) may fail in finding a solution, even though an effective solution exists. Therefore, both the numerical procedures have been embedded into a globalisation strategy. A monotone line search method with Armijo rule has been employed, with a maximum of 10 backtracks for nonlinear iteration [27,28].

As regards the time integration of the whole model (multibody model and contact model; Figure 1), explicit ODE solvers with a variable step and a variable order have been considered [29]. Moreover, during the simulations, the initial conditions for the nonlinear solvers (the Newton–BiCGStab and the Newton–LU) are continually updated in order to speed up the convergence of the solvers and to reduce the computation time. In other words, the solution of the problem at the current time step is used as the initial condition for the solver at the next time step.

5. The multibody model

As benchmark vehicle, the Manchester Benchmark Vehicle has been chosen (Figure 10); the physical and geometrical characteristics of the vehicle can be found in the literature [5,20]. The wheels' back to back distance is 1360 mm.

The multibody model consists of seven rigid bodies: the car body, two bogies and four wheelsets. The secondary suspensions connect the bogies to the car body (Figure 11) and comprise the following elements:

- (1) two springs
- (2) four dampers (lateral and vertical dampers)
- (3) the traction rod
- (4) the roll bar (not visible in the figure)
- (5) two bumpstops

while the primary suspensions connect the wheelsets to the bogies (Figure 12) and comprise two springs and six dampers (longitudinal, lateral and vertical).

Both the stages of suspensions have been modelled by means of three-dimensional viscoelastic force elements (linear and nonlinear). The multibody model of the Manchester Wagon has been implemented in SimMechanics, a Matlab toolbox specifically designed for the multibody

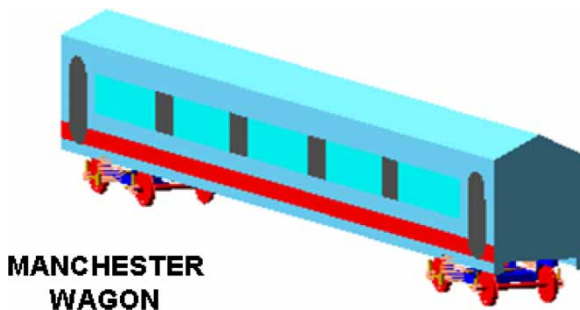


Figure 10. Matlab/Simulink multibody model.

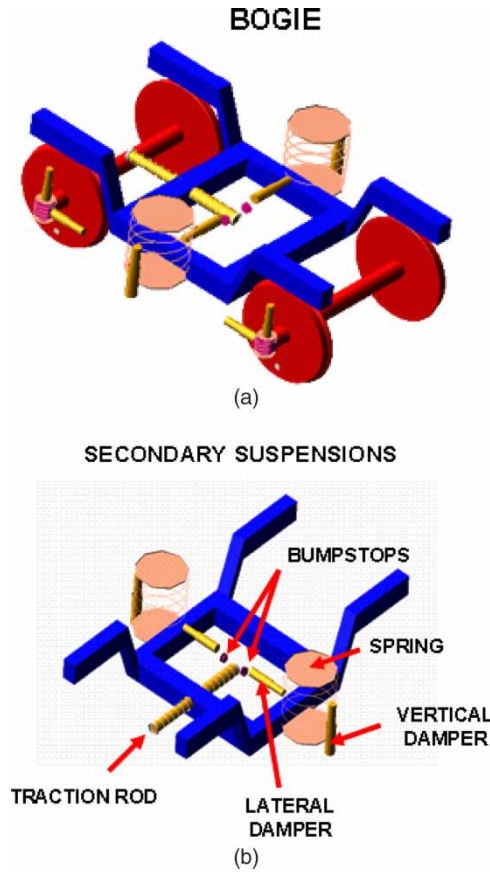


Figure 11. Bogie and secondary suspensions.

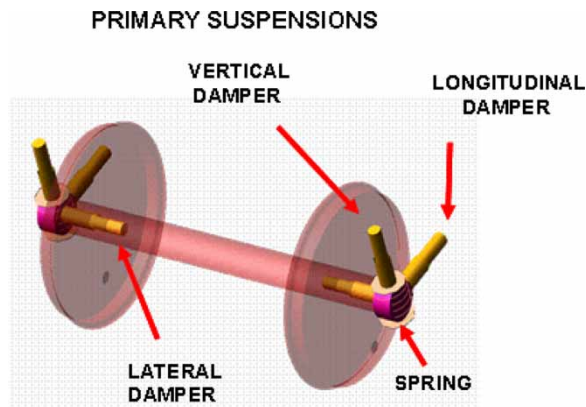


Figure 12. Wheelset and primary suspensions.

dynamics [19]. With respect to the model described in [5,20], a damping coefficient has been added to the anti-roll torsional spring, its value was 94000 N m s/rad, i.e. 10% of the stiffness.

6. The numerical simulations

In order to study the behaviour of the whole model (Figure 1), a large number of dynamic simulations has been performed on many different scenarios obtained by varying the geometrical characteristics of the railway track (Table 1) [5,20,22].

The performance of the model have been evaluated both in terms of numerical efficiency (performance of the numerical procedures and time consumption) and in terms of output accuracy (kinematic variables, contact forces and contact areas).

6.1. Performance of the numerical procedures

In this section, the performance of the numerical procedures described in the previous section will be analysed and compared with each other. By way of example, a typical simulation of the dynamics of the Manchester Wagon will be considered. The simulation has been performed on a curvilinear railway track, the data of which are reported in Table 2 [5,20,22].

The comparison between the numerical methods has been carried out on a machine equipped with an Intel Xeon 2.66 GHz and 8 GB RAM.

In order to compare the *sparse formulation* (27) and the *reduced formulation* (30) of the contact problem, several experimentations have been performed with different ODE solvers such as the ODE23 and the ODE45 [29]. The values of the main numerical parameters relative to the simulation are reported in Table 3 for both the formulations.

Table 1. Characteristics of the railway track: ranges of variation.

| | | |
|-------------------------|------------------|----------------|
| Curvature | K (m^{-1}) | $-0.1-0.1$ |
| Cant angle | β_c (rad) | $-0.15-0.15$ |
| Slope | p (-) | $-0.05 - 0.05$ |
| Laying angle | α_p (rad) | $1/40-1/20$ |
| Velocity | V (km/h) | $0-300$ |
| Friction | μ (-) | $0-0.5$ |
| Transition curve length | (m) | 50 |
| Full curve length | (m) | 100 |

Table 2. Data of the curvilinear track.

| | | |
|--------------|------------------|-----------|
| Curvature | K (m^{-1}) | $-1/1200$ |
| Cant angle | β_c (rad) | 0.0418 |
| Slope | p (-) | 0 |
| Laying angle | α_p (rad) | $1/40$ |
| Velocity | V (km/h) | 162 |
| Friction | μ (-) | 0.3 |

Table 3. Numerical parameter.

| Formulation | Equation (27) | Equation (30) |
|------------------|-------------------|-------------------|
| RelTol/AbsTol | $10^{-8}/10^{-6}$ | $10^{-8}/10^{-6}$ |
| Nonlinear Solver | Newton-BiCGStab | Newton-BiCGStab |
| Tol/MaxitNonlin | $10^{-7}/20$ | $10^{-7}/20$ |
| η /MaxitLin | $0.01/20$ | $0.01/20$ |

Notes: RelTol and AbsTol are the relative and absolute tolerances of the ODE solvers, MaxitNonlin and MaxitLin are the maximum number of nonlinear and linear iterations, Tol is the stopping tolerance (Equation (36)) and η is the forcing term. In particular, the values of the tolerances RelTol, AbsTol and Tol have been chosen in order to assure a sufficient accuracy (in terms of displacements and contact pressures) and, at the same time, to minimise the computational load.

Table 4. Performance of formulation (27) using ODE23.

| Wheel–rail pair | Differential contact model: formulation (27) | | | | | |
|-----------------|--|-----------------|------------|-------------|-----------|----------|
| | CPS | CT: $14^h 21^m$ | IterNonlin | ErrorNonlin | IterLin | ErrorLin |
| 1L | 139,645 | 48.9 ms | 184,266 | 15 | 1,123,071 | 2272 |
| 1R | 139,645 | 43.5 ms | 169,278 | 5 | 969,991 | 1252 |
| 2L | 139,645 | 49.0 ms | 182,673 | 3 | 1,204,867 | 2640 |
| 2R | 139,645 | 43.4 ms | 168,796 | 10 | 1,023,716 | 1122 |
| 3L | 139,645 | 49.5 ms | 185,937 | 5 | 1,201,980 | 2244 |
| 3R | 139,645 | 42.9 ms | 167,353 | 7 | 1,001,942 | 1477 |
| 4L | 139,645 | 50.3 ms | 184,237 | 5 | 1,261,439 | 2177 |
| 4R | 139,645 | 42.2 ms | 164,729 | 8 | 996,849 | 1060 |

Table 5. Performance of formulation (30) using ODE23.

| Wheel–rail pair | Differential contact model: formulation (30) | | | | | |
|-----------------|--|----------------|------------|-------------|---------|----------|
| | CPS | CT: $3^h 46^m$ | IterNonlin | ErrorNonlin | IterLin | ErrorLin |
| 1L | 150,156 | 12.0 ms | 162,111 | 13 | 705,742 | 1428 |
| 1R | 150,156 | 10.7 ms | 148,925 | 4 | 609,546 | 787 |
| 2L | 150,156 | 12.0 ms | 160,709 | 3 | 757,143 | 1659 |
| 2R | 150,156 | 10.6 ms | 148,501 | 9 | 643,307 | 705 |
| 3L | 150,156 | 12.1 ms | 163,581 | 4 | 755,329 | 1410 |
| 3R | 150,156 | 10.5 ms | 147,231 | 5 | 629,624 | 928 |
| 4L | 150,156 | 12.3 ms | 162,085 | 4 | 792,693 | 1368 |
| 4R | 150,156 | 10.3 ms | 144,923 | 7 | 626,424 | 666 |

Tables 4 and 5 summarise the results obtained by using the ODE 23 and relative, respectively, to the *sparse formulation* (27) and to the *reduced formulation* (30). For each wheel–rail contact pair, the following data have been considered:

- (1) the number *CPS* of contact problems solved during the dynamic simulation (equal for all the eight contact pairs)
- (2) the mean computation times *CT* relative to each contact model (the time needed to solve one contact problem) and the total computation time required by the eight contact models
- (3) the total number *IterNonlin* of nonlinear iterations and the convergence errors of the nonlinear solver *ErrorNonlin*
- (4) the total number *IterLin* of linear iterations and the convergence errors of the linear solver *ErrorLin*.

Table 6. Performance of formulation (27) using ODE45.

| Wheel–rail pair | Differential contact model: formulation (27) | | | | | |
|-----------------|--|-----------------|------------|-------------|-----------|----------|
| | CPS | CT: $22^h 16^m$ | IterNonlin | ErrorNonlin | IterLin | ErrorLin |
| 1L | 181,689 | 58.4 ms | 283,334 | 23 | 1,973,568 | 3993 |
| 1R | 181,689 | 52.0 ms | 260,288 | 7 | 1,704,562 | 2201 |
| 2L | 181,689 | 58.5 ms | 280,884 | 5 | 2,117,308 | 4639 |
| 2R | 181,689 | 51.8 ms | 259,547 | 16 | 1,798,972 | 1971 |
| 3L | 181,689 | 59.1 ms | 285,903 | 7 | 2,112,236 | 3943 |
| 3R | 181,689 | 51.2 ms | 257,327 | 9 | 1,760,709 | 2595 |
| 4L | 181,689 | 60.0 ms | 283,289 | 7 | 2,216,722 | 3826 |
| 4R | 181,689 | 50.3 ms | 253,293 | 12 | 1,751,760 | 1862 |

Table 7. Performance of formulation (30) using ODE45.

| Differential contact model: formulation (30) | | | | | | |
|--|---------|------------------------------------|------------|-------------|-----------|----------|
| Wheel-rail pair | CPS | CT: 5 ^h 40 ^m | IterNonlin | ErrorNonlin | IterLin | ErrorLin |
| 1L | 216,225 | 12.5 ms | 259,378 | 21 | 1,129,187 | 2285 |
| 1R | 216,225 | 11.1 ms | 238,280 | 6 | 975,274 | 1259 |
| 2L | 216,225 | 12.5 ms | 257,134 | 5 | 1,211,429 | 2654 |
| 2R | 216,225 | 11.1 ms | 237,602 | 14 | 1,029,291 | 1128 |
| 3L | 216,225 | 12.6 ms | 261,730 | 6 | 1,208,526 | 2256 |
| 3R | 216,225 | 10.9 ms | 235,570 | 8 | 1,007,398 | 1485 |
| 4L | 216,225 | 12.8 ms | 259,336 | 6 | 1,268,309 | 2189 |
| 4R | 216,225 | 10.8 ms | 231,877 | 11 | 1,002,278 | 1066 |

Table 8. Numerical parameter.

| Formulation | Equation (30) |
|------------------|------------------------------------|
| RelTol/AbsTol | 10 ⁻⁸ /10 ⁻⁶ |
| Nonlinear solver | Newton-LU |
| Tol/MaxitNonlin | 10 ⁻⁷ /20 |

Table 9. Performance of the nonlinear solver Newton-LU.

| Wheel-rail pair | CPS | CT: 4 ^h 35 ^m | IterNonlin | ErrorNonlin |
|-----------------|---------|------------------------------------|------------|-------------|
| 1L | 141,147 | 15.3 ms | 137,146 | 11 |
| 1R | 141,147 | 13.6 ms | 125,991 | 3 |
| 2L | 141,147 | 15.3 ms | 135,960 | 3 |
| 2R | 141,147 | 13.6 ms | 125,632 | 8 |
| 3L | 141,147 | 15.5 ms | 138,390 | 3 |
| 3R | 141,147 | 13.4 ms | 124,557 | 4 |
| 4L | 141,147 | 15.7 ms | 137,124 | 3 |
| 4R | 141,147 | 13.2 ms | 122,605 | 6 |

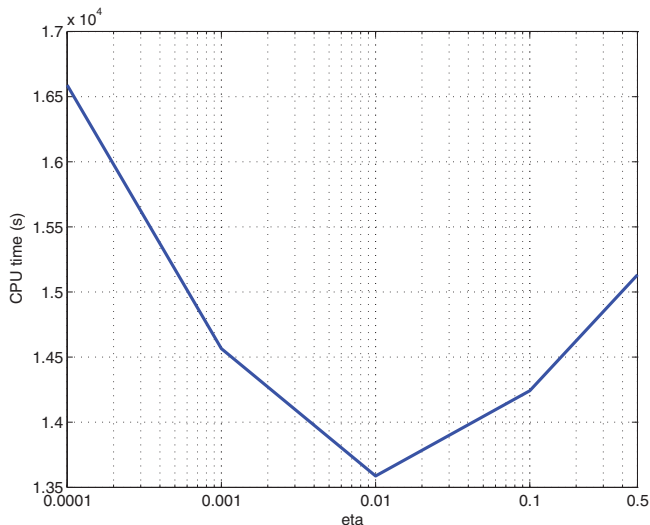


Figure 13. Computation time as a function of the constant forcing term η .

The asymmetry of the data is due to the asymmetry of the railway track (in this case a curve on the right; Table 2). Similarly, Tables 6 and 7 report the same quantities obtained by using the ODE45.

The results show that the *reduced formulation* (30) is more efficient than the *sparse formulation* 27 even though the *reduced formulation* (30) may require a bigger memory consumption (see Section 4.3). In both cases, ODE solvers with low order like ODE23 turned out to be faster than ODE solvers with higher order like ODE45.

Moreover, thanks to the continuous updating of the initial conditions of the nonlinear solver (see Section 4.4), the number of nonlinear and linear iterations (IterNonlin and IterLin) is quite small with respect to the number of contact problems solved CPS while the number of convergence errors (ErrorNonlin and ErrorLin) is negligible ($\leq 1.65\%$).

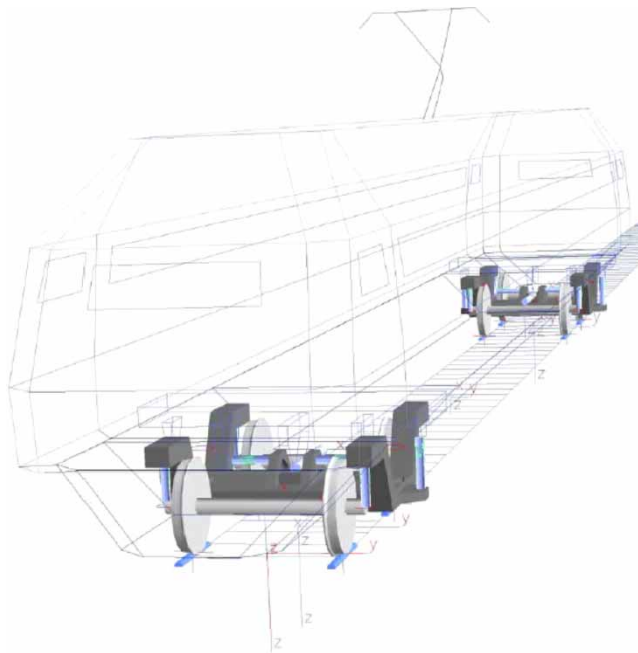


Figure 14. Simpack Rail multibody model.

Table 10. Numerical parameter: Matlab/Simulink model.

| ODE Solver | ODE23 |
|------------------|---------------------------------|
| RelTol/AbsTol | $10^{-8}/10^{-6}$ |
| Contact model | <i>Reduced formulation</i> (30) |
| Nonlinear solver | Newton–BiCGStab |
| Tol/MaxitNonlin | $10^{-7}/20$ |
| η /MaxitLin | 0.01/20 |

Table 11. Numerical parameter: Simpack rail model.

| ODE solver | ODE5 |
|---------------|---------------------------------------|
| Fixed step | $5 * 10^{-4}$ (s) |
| Contact model | Semi-elastic approach (see Section 1) |

As said in the Section 4.4, *reduced formulation* (30) can be also solved by means of the Newton–LU nonlinear solver. Table 9 contains the results obtained through this method. The ODE solver used is ODE23 while the values of the main numerical parameters relative to the simulation are reported in Table 8.

The comparison between the results (Tables 5 and 9) shows that the Newton–BiCGStab method is more efficient than the Newton–LU method in spite of the small dimensions of the discrete problem (30) (the *reduced formulation*). In particular, the computation and the storage of the whole Jacobian at each nonlinear iteration turn out to be quite time-consuming. Concerning the nonlinear iterations *IterNonlin* and the convergence errors *ErrorNonlin* the same considerations of the previous case still hold.

Finally, as regards the *reduced formulation* (30), some experimentations have been performed in order to justify the optimal choice of the constant forcing term $\eta = 10^{-2}$ in the nonlinear solver Newton–BiCGStab. The ODE solver employed is always ODE23

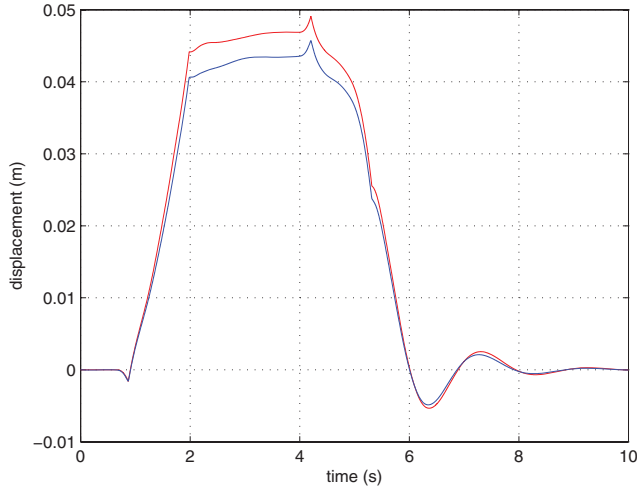


Figure 15. Car body: lateral displacement of the centre of mass y_{CB}^R .

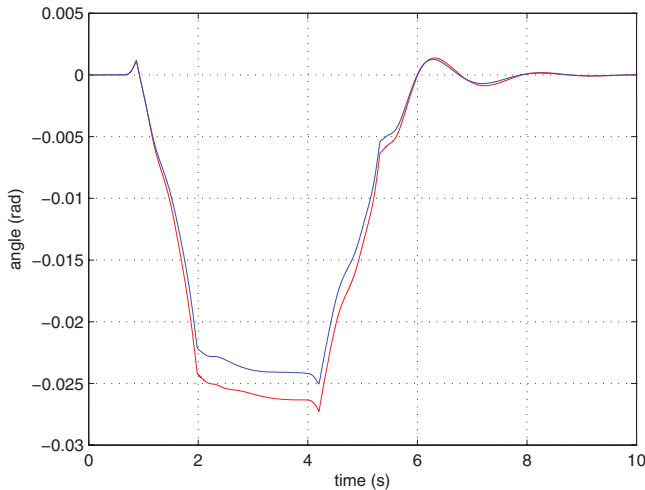


Figure 16. Car body: roll angle ψ_{CB}^R .

while the other numerical parameters are summarised in Table 3. The results, in terms of computation time, have been reported in Figure 13 for the following values of the parameter η : $\eta = 0.5, 10^{-1}, 10^{-2}, 10^{-3}, 10^{-4}$.

6.2. The multibody model implemented in Simpack Rail

The 3D multibody model of the same vehicle has been then implemented also in Simpack Rail, a commercial multibody software for railway vehicles widely tested and validated (Figure 14) [20,21].

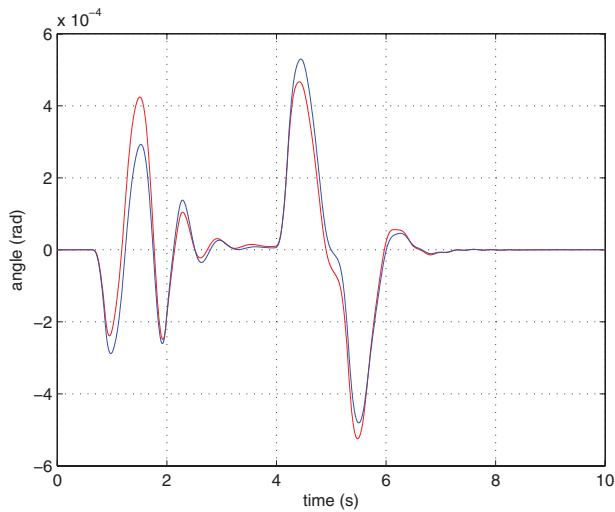


Figure 17. Car body: yaw angle ψ_{CB}^R .

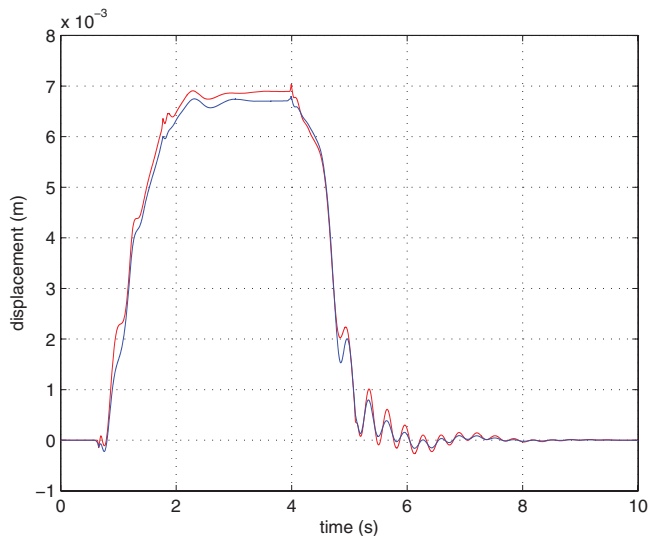


Figure 18. Bogie: lateral displacement of the centre of mass y_B^R .

This time the model is equipped with a standard contact model based on the semi-elastic approach and able to consider the multiple contact (see Section 1) [4–10]. The comparison between the results obtained by the Matlab/Simulink model and those obtained by the Simpack ail model has allowed an accurate and reliable validation of the new contact model.

6.3. The dynamical simulations

In order to compare the performance of the Matlab/Simulink model and the Simpack Rail model in terms of accuracy, a simulation performed on the same curvilinear railway track

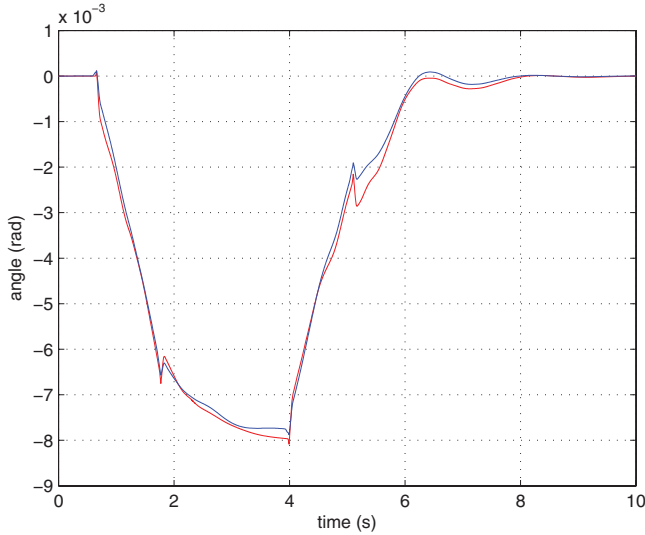


Figure 19. Bogie: roll angle φ_B^R .

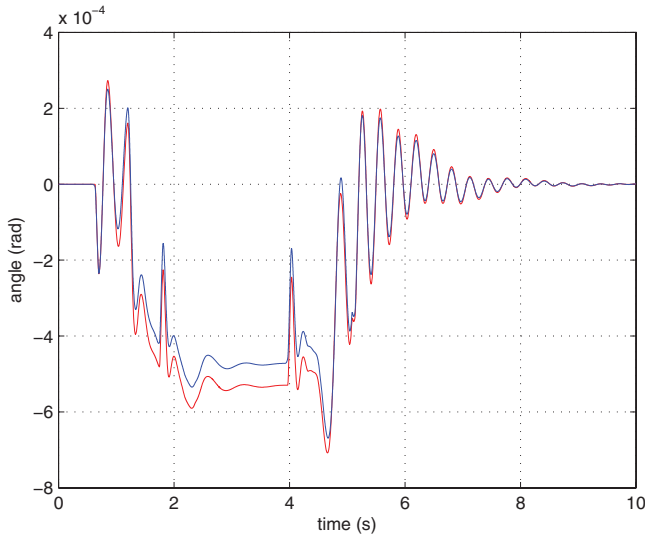


Figure 20. Bogie: yaw angle ψ_B^R .

described in the Section 6.1 will be considered by way of example (for the data of the track, see Table 2) [5,20,22].

The numerical parameters relative to the Matlab/Simulink model have been chosen starting from the results obtained in the Section 6.1 (Table 10). In particular, it is equipped with the contact model based on the *reduced formulation* (30). Similarly, the numerical parameters relative to the Simpack Rail model are briefly summarised in Table 11. The comparison between the models has been carried out on a machine provided with an Intel Xeon 2.66 GHz and 8 GB RAM.

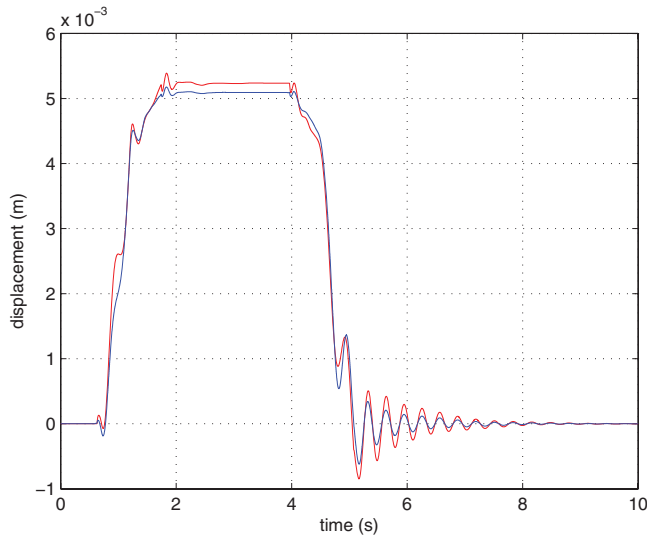


Figure 21. Wheelset: lateral displacement of the centre of mass y_W^R .

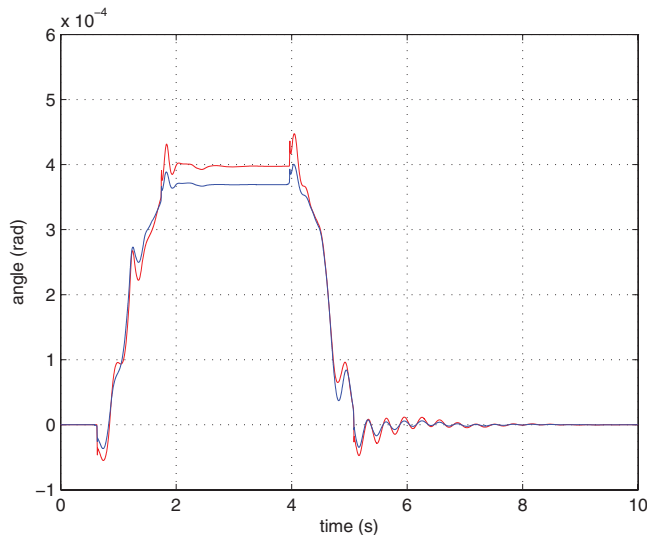


Figure 22. Wheelset: roll angle ϕ_W^R .

Downloaded By: [Malvezzi, Monica] At: 09:55 11 May 2011

Among all the outputs evaluated by the models (kinematic variables, internal forces, contact forces and contact areas), for the sake of simplicity only, the time histories of the following quantities will be reported.

- (1) The lateral displacement of the centre of mass, the roll angle and the yaw angle of the car body ($y_{CB}^R, \varphi_{CB}^R, \psi_{CB}^R$), of the front bogie ($y_B^R, \varphi_B^R, \psi_B^R$) and of the front wheelset of this bogie ($y_W^R, \varphi_W^R, \psi_W^R$) all expressed in the reference system $O_R x_R y_R z_R$.
- (2) The longitudinal, lateral and vertical components of the resultant contact forces on the left and right wheels of the considered wheelset (respectively, $T_{lw}^{xR}, Y_{lw}^R, Q_{lw}^R$ and $T_{rw}^{xR}, Y_{rw}^R, Q_{rw}^R$) always expressed in the system $O_R x_R y_R z_R$.

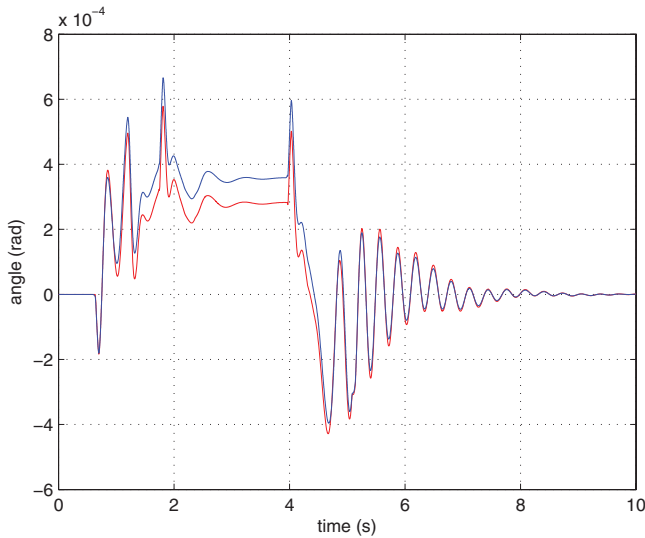


Figure 23. Wheelset: yaw angle ψ_W^R .

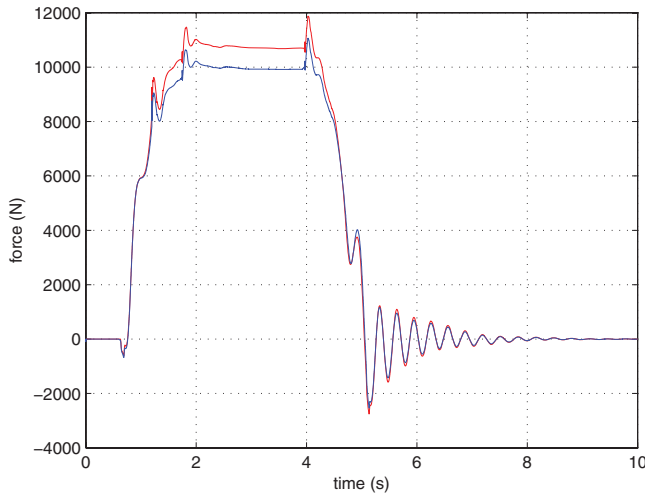


Figure 24. Resultant contact force on the left wheel: longitudinal component T_{lw}^{xR} .

- (3) The real contact areas on the left and right wheel surfaces (A_{wLC} and A_{wRC}) and on the left and right rail surfaces (A_{rLC} and A_{rRC}) respectively expressed in the systems $O_W x_W y_W z_W$ and $O_R x_R y_R z_R$.

The kinematic variables relative to the car body are represented in Figures 15–17 while the same variables relative to the bogie and to the wheelset are reported in Figures 18–23. The Matlab/Simulink quantities are plotted in blue while the Simpack Rail quantities in red.

The analysis of the results shows, as regards the kinematic variables, a good agreement between the Matlab/Simulink model and the Simpack Rail model. The components of the resultant contact forces on the left and right wheels are reported in Figures 24–29 (in blue the Matlab/Simulink quantities and in red the Simpack Rail quantities).

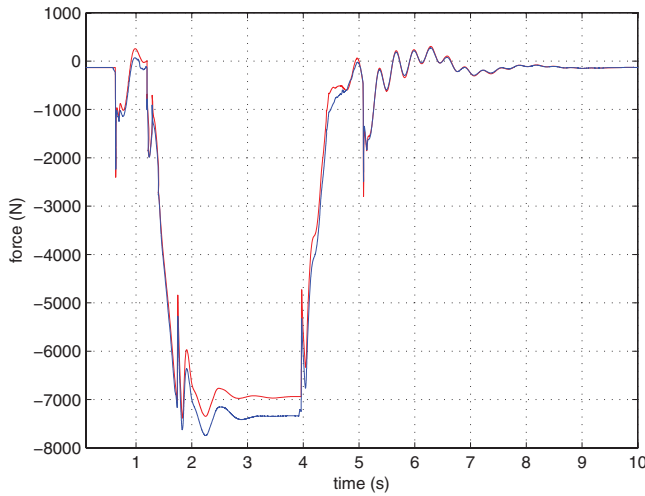


Figure 25. Resultant contact force on the left wheel: lateral component Y_{lw}^R .

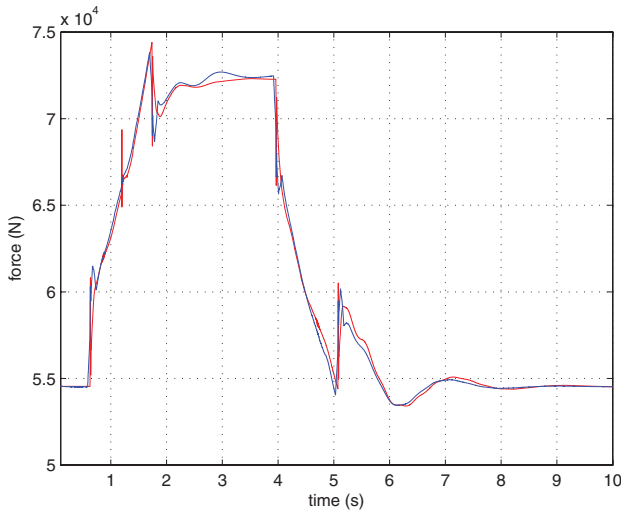


Figure 26. Resultant contact force on the left wheel: vertical component Q_{lw}^R .

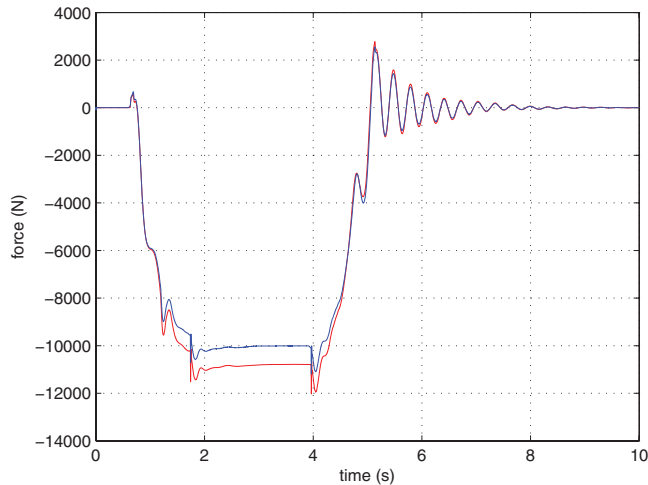


Figure 27. Resultant contact force on the right wheel: longitudinal component T_{rw}^{xR} .

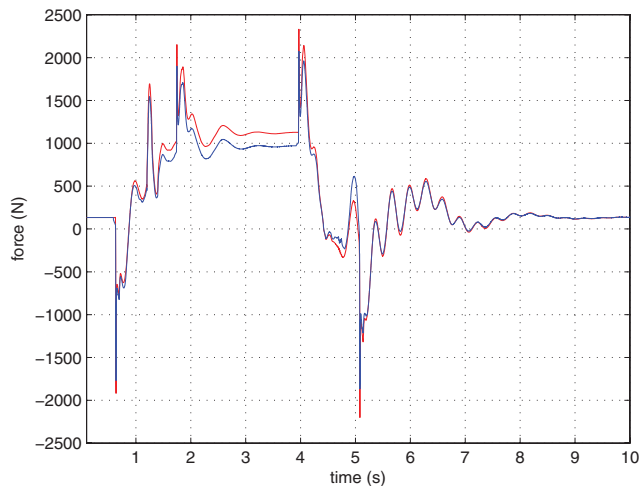


Figure 28. Resultant contact force on the right wheel: lateral component Y_{rw}^R .

The agreement between the models turns out to be good also in terms of resultant contact forces. Finally, the real contact areas on the wheel and rail surfaces are represented. In order to give a clear and effective description of the motion of the contact areas calculated by the Matlab/Simulink model, a lateral section of the contact patches has been plotted on cylindrical surfaces obtained from the wheel and rail profiles (generating profiles) and as long as the distance travelled by the vehicle. Concerning the Simpack Rail model (equipped with a standard contact model), the position of the contact points has been plotted. In Figures 30 and 31 are reported the contact areas on the left and right wheel surfaces while in Figures 32 and 33 on the left and right rail surfaces. The Matlab/Simulink quantities are in blue while the Simpack Rail quantities in black.

As can be seen in the previous figures, during the curve the contact areas calculated by the Matlab/Simulink model on the left wheel and rail surfaces are made up of two disjoint parts (in other words, a multiple contact is present). On the other hand, also the Simpack Rail model

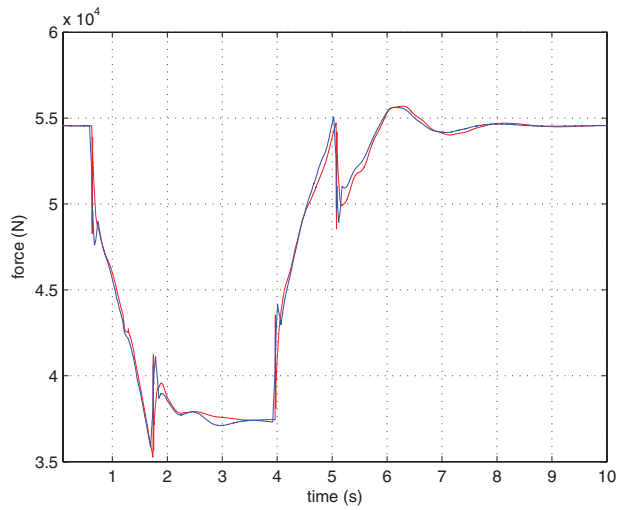


Figure 29. Resultant contact force on the right wheel: vertical component Q_w^R .

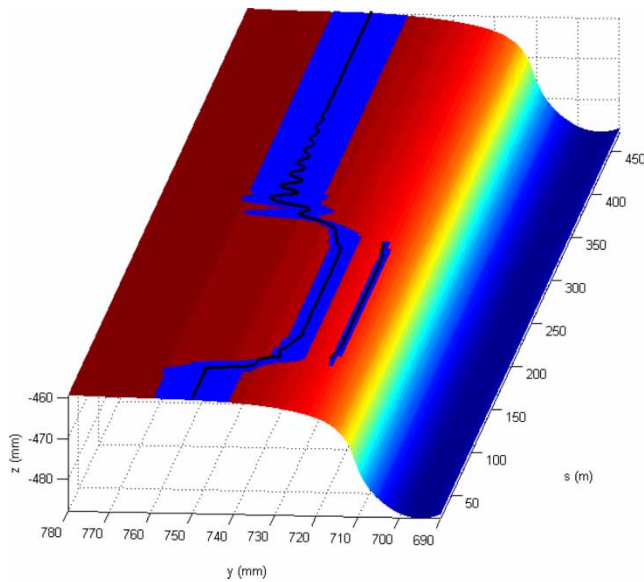


Figure 30. Lateral section of contact area A_{wIC} on the left wheel surface.

detects, during the curve, the presence of a second contact point on the left wheel and rail; in particular the contact points are always contained within the different disjoint parts of the contact areas estimated by the Matlab/Simulink model. From this point of view, there is a good agreement between the models.

The proposed model depends on several parameters, for example, the factious stiffness introduced in Equation (16), the shape and dimension of the FEM discretisation, the form functions etc. The results presented in this section have been obtained with linear tetrahedral elements, that typically are rather stiff, and then lead to smaller contact patches.

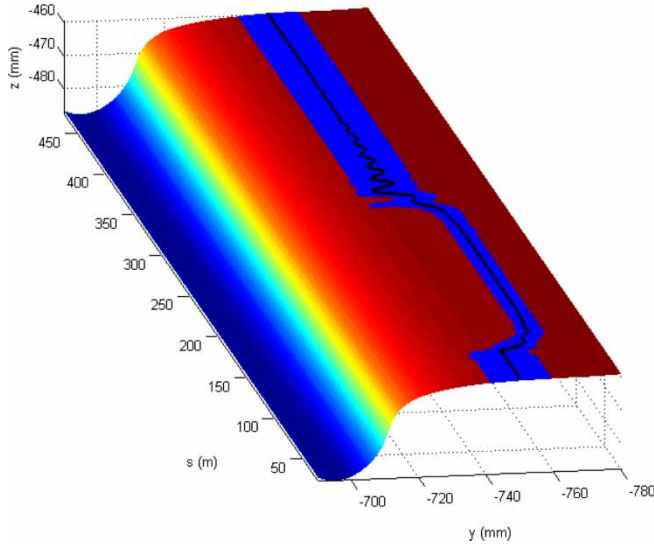


Figure 31. Lateral section of contact area A_{wrC} on the right wheel surface.

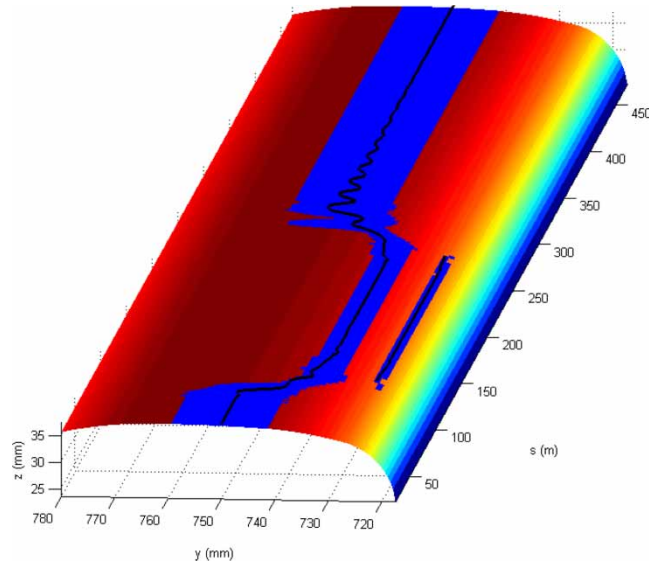


Figure 32. Lateral section of contact area A_{rlC} on the left rail surface.

In conclusion it is useful to observe as the stability of the Matlab/Simulink model and the quasi-total absence of numerical noise highlight the accuracy and the reliability of the new contact model.

Finally, the total computation time $T_g = 4^h32^m$ required from the whole model (multibody model and the eight contact models) has been reported in Figure 34. The time T_g has been compared with the total computation time $T_c = 3^h46^m$ required from the eight contact models (Table 5). The numerical results refer to the simulation considered in this paragraph (Tables 2 and 10).

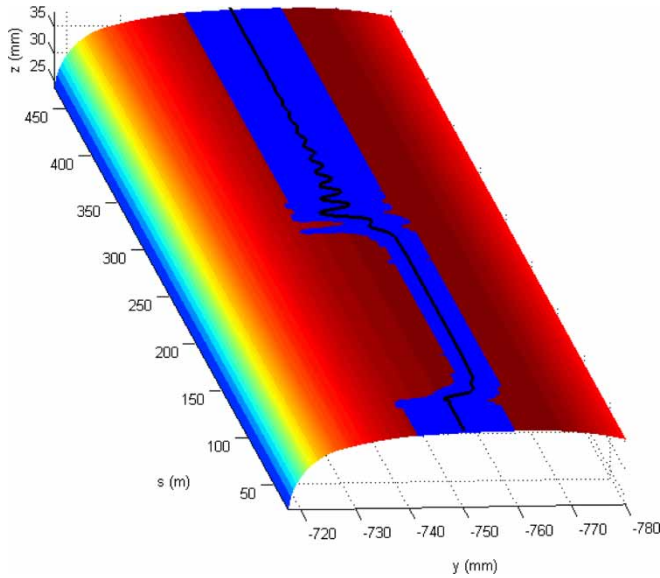


Figure 33. Lateral section of contact area $A_{\pi C}$ on the right rail surface.

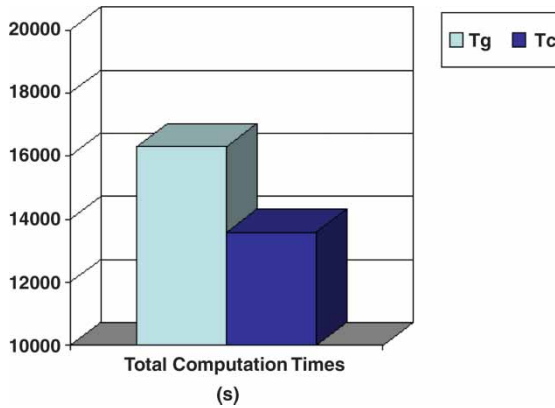


Figure 34. Total computation times required from the whole model T_g and the contact models T_c .

In the analysed case, the time required from the eight contact models is approximately the 83% of the time required from the whole model.

7. Conclusions and further developments

In this work, the authors presented an innovative elastic wheel–rail contact model with the aim of achieving a better integration between multibody and differential modelling. Owing to the high computational load, this kind of integration is almost absent in the literature, especially in the railway field; however, it is very important because only the differential modelling allows an accurate analysis of the contact phenomena while the multibody modelling is the standard in the study of the railway dynamics.

Downloaded By: [Malvezzi, Monica] At: 09:55 11 May 2011

The contact model has been inserted within the multibody model of a benchmark railway vehicle (the Manchester Benchmark Vehicle) in order to obtain a complete model of the wagon. The whole model has been implemented in the Matlab/Simulink environment.

The multibody model of the same vehicle (this time equipped with a standard contact model based on the semi-elastic approach) has been then implemented also in Simpack Rail, a commercial multibody software for railway vehicles widely tested and validated.

Finally, numerical simulations of the vehicle dynamics have been carried out on many different railway tracks. The comparison between the results obtained by the Matlab/Simulink and the Simpack Rail models has allowed an accurate and reliable validation of the new contact model.

The performances of the Matlab model turned out to be good both in terms of output accuracy (kinematic variables, contact forces and contact areas) and in terms of numerical efficiency (performances of the numerical algorithms and time consumption) and satisfy all the specifics reported in the introduction.

As regards the further developments, many optimisations of the differential contact model are scheduled for the future. The improvements will regard especially the FEM techniques used to discretise the contact problem. In particular, new mesh generation algorithms and new nonlinear shape functions will be examined. These techniques assure a better accuracy in the description of the local contact phenomena but increase the dimension of the discrete problem and consequently the computational load and the memory consumption.

In order to reduce the computation time, the contact model will be implemented in programming environments like C/C++ and FORTRAN by means of Matlab S function; moreover, new Matlab toolboxes regarding the distributed computing will be employed.

The future developments will concern also the online implementation of the contact model within commercial multibody softwares such as Simpack Rail. To this end, suitable user routine will be used. A cooperation is currently in progress with INTEC GmbH, the company that produces the software Simpack Rail, in order to develop innovative toolboxes specifically designed for the wheel–rail contact.

Finally, the contact model described in this work will be employed inside new wear models with the aim of predicting the evolution of the worn wheel and rail profiles.

References

- [1] A.A. Shabana and J.R. Sany, *An augmented formulation for mechanical systems with non-generalized coordinates: Application to rigid body contact problems*, Nonlinear Dyn. 24 (2001), pp. 183–204.
- [2] S. Iwnicki, *Simulation of wheel–rail contact forces*, Fatigue Fract. Eng. Mater. Struct. 26 (2003), pp. 887–900.
- [3] J. Pombo and J. Ambrosio, *Dynamic analysis of a railway vehicle in real operation conditions using a new wheel–rail contact detection model*, Int. J. Veh. Syst. Model. Test. 1 (2005), pp. 79–105.
- [4] J.J. Kalker, *Three-dimensional Elastic Bodies in Rolling Contact*, Kluwer Academic Publishers, Dordrecht, The Netherlands, 1990.
- [5] R.V. Dukkipati and J.R. Amyot, *Computer Aided Simulation in Railway Dynamics*, Dekker, New York, 1988.
- [6] O. Polach, *Creep forces in simulations of traction vehicles running on adhesion limit*, Wear 258 (2005), pp. 992–1000.
- [7] A.A. Shabana, K.E. Zaazaa, J.L. Escalona, and J.R. Sany, *Development of elastic force model for wheel/rail contact problems*, J. Sound Vib. 269 (2004), pp. 295–325.
- [8] M. Malvezzi, E. Meli, S. Falomi and A. Rindi, *Determination of wheel–rail contact points with semianalytic methods*, Multibody Syst. Dyn. 20(4) (2008), pp. 327–358.
- [9] J. Auciello, E. Meli, S. Falomi and M. Malvezzi, *Dynamic simulation of railway vehicles: Wheel–rail contact analysis*, Veh. Syst. Dyn. 47(7) (2009), pp. 867–899.
- [10] S. Falomi, M. Malvezzi, E. Meli and M. Rinchi, *Multibody modelling of railway vehicles: Innovative algorithms for the detection of wheel–rail contact points*, Multibody Dynamics 2009 (ECCOMAS), Varsavia, Polonia, 2009.
- [11] G. Duvaut and J.L. Lions, *Les Inequations en Mecanique et en Physique*, Dunod, Paris, France, 1972.
- [12] K.L. Johnson, *Contact Mechanics*, Cambridge University Press, Cambridge, UK, 1985.

- [13] N. Kikuchi and J.T. Oden, *Contact Problems in Elasticity*, SIAM Studies in Applied Mathematics, SIAM Books, Philadelphia, PA, 1988.
- [14] P. Wriggers, *Computational Contact Mechanics*, John Wiley & Sons, Hoboken, NJ, 2002.
- [15] O. Zienkiewicz, *The Finite Element Method in Engineering Science*, McGraw-Hill, NY, 1988.
- [16] A. Klarbring, *A mathematical programming approach to 3D contact problems with frictions*, Comput. Methods Appl. Mech. Eng. 58 (1986), pp. 175–200.
- [17] G. Dhatt and G. Touzot, *The Finite Element Method Displayed*, John Wiley & Sons, Hoboken, NJ, 1984.
- [18] M. Busquet, H. Chollet, L. Baillet, C. Dagorn, J.B. Ayasse and Y. Bertheir, *From railway dynamics to wheel/rail contact mechanics, an approach for the modelling of the wheel/rail contact: Elasto-plastic response of the railhead*, Proc. Instn Mech. Eng., Part F, J. Rail Rapid Transit 220 (2006), pp. 189–200.
- [19] Official Site of The MathWorks, Natick, Massachusetts, 2009. Available at <http://www.mathworks.com>
- [20] S. Iwnicki, *The Manchester Benchmarks for Rail Vehicle Simulators*, Swets & Zeitlinger, Lisse, The Netherlands, 1999.
- [21] Official Site of the INTEC GmbH, <http://www.simpack.com>, Gilching, Germany, 2009.
- [22] C. Esveld, *Modern Railway Track*, Delft University of Technology, Delft, The Netherlands, 2001.
- [23] G. Vicuna, *Organizzazione e Tecnica Ferroviaria*, CIFI, Roma, Italy, 1986.
- [24] M. doCarmo, *Differential Geometry of Curves and Surfaces*, Prentice-Hall, Upper Saddle River, NJ, 1976.
- [25] R.S. Dembo, S.C. Eisenstat, and T. Steihaug, *Inexact Newton methods*, SIAM J. Numer. Anal. 19 (1982), pp. 400–408.
- [26] C. Kelley, *Iterative Methods for Linear and Nonlinear Equations*, SIAM, Philadelphia, PA, 1995.
- [27] Y. Saad, *Iterative Methods for Sparse Linear Systems*, SIAM, Philadelphia, PA, 2003.
- [28] J. Nocedal and S. Wright, *Numerical Optimization*, Springer Series in Operation Research, Springer, Berlin, Germany, 1999.
- [29] L.F. Shampine and M.W. Reichelt, *The MATLAB ODE Suite*, SIAM J. Scient. Comput. 18 (1997), pp. 1–22.